nature

https://doi.org/10.1038/s41586-020-2600-6

Accelerated Article Preview

Association of COVID-19 inflammation with activation of the C5a–C5aR1 axis

Received: 29 April 2020

Accepted: 23 July 2020

Accelerated Article Preview Published online 29 July 2020

Cite this article as: Carvelli, J. et al. Association of COVID-19 inflammation with activation of the C5a–C5aR1 axis. *Nature* https://doi.org/10.1038/s41586-020-2600-6 (2020).

Julien Carvelli, Olivier Demaria, Frédéric Vély, Luciana Batista, Nassima Chouaki Benmansour, Joanna Fares, Sabrina Carpentier, Marie-Laure Thibult, Ariane Morel, Romain Remark, Pascale André, Agnès Represa, Christelle Piperoglou, the Explore COVID-19 IPH group, the Explore COVID-19 Marseille Immunopole group, Pierre Yves Cordier, Erwan Le Dault, Christophe Guervilly, Pierre Simeone, Marc Gainnier, Yannis Morel, Mikael Ebbo, Nicolas Schleinitz & Eric Vivier

Article

Association of COVID-19 inflammation with activation of the C5a–C5aR1 axis

https://doi.org/10.1038/s41586-020-2600-6

Received: 29 April 2020

Accepted: 23 July 2020

Published online: 29 July 2020

Julien Carvelli[1,2,11], Olivier Demaria[3,11], Frédéric Vély[4,5,11], Luciana Batista[3], Nassima Chouaki Benmansour[6,10], Joanna Fares[3], Sabrina Carpentier[3], Marie-Laure Thibult[3], Ariane Morel[3], Romain Remark[3], Pascale André[3], Agnès Represa[3], Christelle Piperoglou[4,5], the Explore COVID-19 IPH group*, the Explore COVID-19 Marseille Immunopole group[2,4,6,10]*, Pierre Yves Cordier[6], Erwan Le Dault[6], Christophe Guervilly[2,7], Pierre Simeone[2,8], Marc Gainnier[1,2], Yannis Morel[3], Mikael Ebbo[4,9], Nicolas Schleinitz[4,9] & Eric Vivier[3,4,5]✉

Coronavirus disease 2019 (COVID-19) is a new pandemic disease caused by infection with severe acute respiratory syndrome coronavirus 2 (SARS-CoV-2)[1]. The C5a anaphylatoxin and its receptor C5aR1 (CD88) play a key role in the initiation and maintenance of several inflammatory responses, by recruiting and activating neutrophils and monocytes in the lungs[1]. We provide a longitudinal analysis of immune responses, including immune cell phenotyping and assessments of the soluble factors present in the blood and broncho-alveolar lavage fluid (BALF) of patients at various stages of COVID-19 severity: paucisymptomatic, pneumonia and acute respiratory distress syndrome (ARDS). We report an increase in soluble C5a levels proportional to COVID-19 severity and high levels of C5aR1 expression in blood and pulmonary myeloid cells, supporting a role for the C5a-C5aR1 axis in the pathophysiology of ARDS. Anti-C5aR1 therapeutic monoclonal antibodies (mAbs) prevented C5a-mediated human myeloid cell recruitment and activation, and inhibited acute lung injury (ALI) in human C5aR1 knockin mice. These results suggest that C5a-C5aR1 axis blockade might be used as a means of limiting myeloid cell infiltration in damaged organs and preventing the excessive lung inflammation and endothelialitis associated with ARDS in COVID-19 patients.

Most COVID-19 patients present only a few mild symptoms, but about 15% of patients progress to severe pneumonia, and about 5% develop ARDS, for which effective therapeutic strategies are urgently required[2]. The immune system plays a dual role in COVID-19, contributing to both virus elimination and ARDS development[2]. A detailed characterization of the immune responses occurring during disease progression from mild to severe forms is thus crucial to an understanding of the ways in which we could manipulate immunity to propose new therapies. In particular, given the urgent need for effective treatments for pneumonia in COVID-19 patients, dissection of the immune responses occurring during the course of COVID-19 could lead to the repurposing of approved immunomodulatory drugs and candidate drugs already tested in clinical trials. We thus monitored immune parameters in a cohort of 82 individuals: 10 healthy controls (HC), 10 paucisymptomatic (pauci) COVID-19 patients, 34 patients with pneumonia (pneumo) and 28 patients with ARDS due to SARS-CoV-2 (Supplementary Table 1). We focused on molecular pathways that could block the overt inflammation associated with ARDS.

Disease severity was associated with an increase in the amounts of plasma C-reactive protein (CRP) and inflammatory cytokines, such as interleukin-6 (IL-6), and the chemokines CCL4 (macrophage inflammatory protein-1β), CCL2 (monocyte chemoattractant protein 1) and CXCL9 (monokine induced by gamma interferon), produced by and acting on myeloid cells (Fig. 1a). These results confirmed earlier observations on the "cytokine storm" that develops in patients with severe COVID-19[3]. The ability of plasma from patients to neutralize SARS-CoV-2 virus is also correlated with disease severity (Extended Fig. 1a), consistent with previous data reporting higher titers of anti-SARS-CoV-2 antibodies in patients with severe COVID-19[4].

We decided to focus on the complement factor C5a, which mediates strong chemoattraction and the activation of myeloid cells[5], and plays well-documented roles specifically in lung inflammation and injury[6]. The complement cascade plays a crucial role in pathogen sensing and clearance, and inflammation[7], and involves several components, including cell surface receptors and soluble regulators. In the final phase of the response, the membrane attack complex (MAC: C5b9), and the

[1]Assistance Publique des Hôpitaux de Marseille, Hôpital de la Timone, Réanimation des Urgences, Marseille, France. [2]Aix Marseille Univ, Marseille, France. [3]Innate Pharma, Marseille, France. [4]Aix Marseille Univ, CNRS, INSERM, CIML, Marseille, France. [5]Assistance Publique des Hôpitaux de Marseille, Hôpital de la Timone, Immunology, Marseille Immunopole, Marseille, France. [6]Hôpital d'Instruction des Armées Laveran, Marseille, France. [7]Assistance Publique des Hôpitaux de Marseille, Hôpital Nord, Réanimation des Détresses Respiratoires et Infections Sévères, Aix-Marseille Université, Marseille, France. [8]Assistance Publique des Hôpitaux de Marseille, Hôpital de la Timone, Réanimation Polyvalente, Aix-Marseille Université, Marseille, France. [9]Assistance Publique des Hôpitaux de Marseille, Hôpital de la Timone, Internal Medicine, Marseille, France. [10]Assistance Publique des Hôpitaux de Marseille, Marseille, France. [11]These authors contributed equally: Julien Carvelli, Olivier Demaria, Frédéric Vély. *Lists of authors and their affiliations appear at the end of the paper. ✉e-mail: vivier@ciml.univ-mrs.fr

potent chemoattractants and inflammatory mediators C3a and C5a are generated. The MAC forms transmembrane channels on the surface of pathogen cells, disrupting the cell membrane and leading to cell death. The C3a and C5a proteins regulate inflammation by binding to their receptors, C3aR and C5aR1[8]. Exaggerated complement activation contributes to the pathogenesis of many inflammatory and immune diseases[5]. Many studies of the lung epithelium have reported depositions of complement components during inflammation and suggested that the systemic activation of complement leads, via C5a, to neutrophil recruitment, activation, and adhesion to the pulmonary endothelium, resulting in cell damage, and subsequent ALI and ARDS, which may be fatal[1,6,9]. We observed an increase in plasma C5a levels proportional to COVID-19 severity (Fig. 1b). C5a levels increased in a few patients in the paucisymptomatic group, and was significantly higher than those in HC in both groups displaying lung damage: the pneumonia and ARDS groups (Fig. 1b). The longitudinal follow-up of COVID-19 patients revealed that the upregulation of circulating C5a levels was maintained for at least 10 days after the inclusion of the patients in our cohort (Extended Fig. 1b). The higher levels of C5a in the patients with the most severe symptoms suggests a role for this anaphylatoxin in the cytokine storm occurring in patients developing ARDS. Increased systemic and local complement pathway activity was confirmed by transcriptomic analysis on the peripheral blood of COVID-19 patients, showing an upregulation of *C1Q* and *C2* expression (Extended Fig. 1c) and by the presence of C5b9, as shown by immunostaining, in lung sections from COVID-19 patients (Extended Fig. 1d). Consistent with these results, high levels of C5a in COVID-19 patients have recently been reported to be a consequence of overt activation of the complement cascade by the SARS-CoV-2 N-protein[10]. Furthermore, anti-SARS-CoV-2 antibodies[4] and CRP may also contribute to the activation of the classical pathway of complement during COVID-19. Thus, factors triggering activation of the lectin and the classical complement pathway are upregulated in COVID-19 and may sustain the high level of C5a detected.

We found that COVID-19 was associated with peripheral blood neutrophilia (Fig. 2a), as reported in other cohorts[11]. No major changes were observed in the total peripheral blood monocyte population, but the proportion of conventional $CD14^+CD16^-$ monocytes increased, whereas the proportion of inflammatory $CD14^{low}CD16^+$ monocytes decreased in peripheral blood (Fig. 2b), consistent with the possibility of inflammatory monocytes leaving the bloodstream and homing to tissues. This hypothesis was supported by transcriptomic analyses on symptomatic COVID-19 patients, which revealed not only an increase in transcript levels for genes such as *IRAK3*, *MS4A6A*, *CD33*, *CD300C*, *VCAN*, *CD1D*, *CCR1*, *OAS1*, *CD163* and *C3AR1* in peripheral blood monocytes, but also an upregulation of macrophage and monocyte transcriptomic signatures in inflamed lungs (Extended Fig. 1c).

Both circulating neutrophils and monocytes displayed strong C5aR1 expression in healthy individuals that was also observed in the various groups of COVID-19 patients (Fig. 2c). Longitudinal immune-monitoring follow-up of patients with pneumonia and ARDS showed that the levels of C5aR1 molecules remained stable on circulating neutrophils and monocytes, or even increased during the course of the disease (Extended Fig. 2a). Consistent with the inflammatory function of C5a[12], and the expression of C5aR1 on monocytes, C5a increased the production of the inflammatory cytokines IL-6, TNFα and CCL2 induced by LPS on purified blood monocytes isolated from the various groups of COVID-19 patients (Fig. 2d). C5a also increased the production of cytokines by the monocytes of COVID-19 patients following stimulation with R848, which activates the TLR7/TLR8 MyD88-dependent signaling pathway, mimicking the single-stranded RNA of SARS-CoV-2 (Fig. 2d).

Given that severe COVID-19 is associated with lung disease, we then focused on this organ. C5a was detected in the BALF of ARDS COVID-19 patients (Fig. 3a). Inflammatory cytokines, such as CXCL8, CXCL9, CCL2, and, to a lesser extent, CCL4, IL-6, TNF-α and IL-1β, were also detected in these samples (Fig. 3a). Large numbers of neutrophils and monocytes were found in the BALF of ARDS COVID-19 patients and these cells expressed C5aR1 (Fig. 3b). In addition, the analysis of single-cell RNAseq data from healthy controls and ARDS COVID-19 patients[13] revealed major changes in the myeloid cell population infiltrating the lungs during the course of SARS-CoV-2 infection. Indeed, the major myeloid cell subset (subset A) in healthy controls and the major myeloid cell subset (subset B) in ARDS COVID-19 patients were clearly different (Fig. 3c and Extended Fig. 3a and 3b). The cells of subset B were characterized by higher levels of transcripts for inflammatory cytokine genes, such as *CXCL8*, *CCL2*, *CCL4*, *CXCL9*, *TNF-α* and *IL-6* (Fig. 3d). A slight upregulation was observed in subset B, but both myeloid cell subsets expressed *C5aR1* (Fig. 3d). A multiplex immunohistochemistry analysis of lungs from deceased ARDS COVID-19 patients confirmed pulmonary infiltration with $CD68^+CD163^+$ macrophages, a substantial proportion of which expressed C5aR1 (Extended Fig. 3c; right panel), relative to lung tissue from a control without COVID-19 (Extended Fig. 3c; left panel). It is becoming increasingly clear that severe COVID-19 is associated with the spread of the virus through the epithelial barrier and endothelialitis[14,15]{Copin, 2020 #227}. We observed obliterating endarteritis associated with an accumulation of $C5aR1^+$ macrophages around the arteries and in the thrombus (Extended Fig. 3d). Together with the high levels of C5a in symptomatic COVID-19 patients, these data support the hypothesis that C5a production leads to the chemo-attraction and activation of myeloid cells in the lungs, and contributes to the overt release of inflammatory cytokines. As C5a can also promote the secretion of CCL2, a strong chemoattractant for monocytes, C5a may also promote the recruitment of inflammatory cells indirectly, through the induction of other chemokines. It is also possible that the vasculitis associated with severe COVID-19 is linked to the production of C5a, as other types of vasculitis, such as anti-neutrophil cytoplasmic antibody (ANCA)-associated vasculitis, are mediated by C5a[16].

Based on this hypothesis, we reasoned that C5a-C5aR1 axis blockade could be proposed as a potential therapeutic strategy for severe COVID-19. Several molecules could be repurposed to this end, including anti-C5 mAbs, anti-C5a mAbs and C5aR1 antagonists. We focused on avdoralimab, a fully human Fc-silent mAb against C5aR1 that prevents its binding to C5a. *In vitro*, C5aR1 blockade with avdoralimab inhibited C5a-induced neutrophil activation, as shown by evaluation of the induction of CD11b expression at the cell surface (Fig. 4a). The C5a-mediated upregulation of CD11b was also inhibited by other C5aR1 antagonists or anti-C5a mAbs (Extended Fig. 4a). Avdoralimab blocked the neutrophil activation induced by very high concentrations of C5a (Fig. 4b). Concerning the infiltration of $C5aR1^+$ myeloid cells in the inflamed lungs of patients with severe COVID-19, avdoralimab also inhibited the C5a-induced migration of neutrophils *in vitro* (Fig. 4c). We then investigated whether avdoralimab could block the development of ALI in a mouse model. As avdoralimab targets human C5aR1, we used mice with a knock in for human C5aR1 (HuC5aR1 KI mice)[18] displaying huC5aR1 expression exclusively on $CD11b^+$ myeloid cells (Extended Fig. 4b). HuC5aR1 KI mice receiving an intranasal instillation of recombinant human C5a developed acute lung inflammation and injury 18 hours post injection, as shown by the infiltration of $CD45^+$ immune cells including $Ly6G^+Ly6C^+$ neutrophils and $Ly6G^-Ly6C^+$ monocytes into the lung (Fig. 4d) and the release of albumin in BALF (Fig. 4e), a marker of alveolar-capillary permeability and lung injury. ALI was confirmed by histopathology analysis of lung sections that revealed massive inflammatory cell infiltration, alveolar hemorrhage and thickening of alveolar walls in lungs of C5a-treated mice (Extended Fig. 4c), as previously described[9]. Avdoralimab blocked the infiltration of both cell types (Fig. 4d), prevented albumin release in BALF (Fig. 4e) and limited C5a-induced ALI histopathological features (Extended Fig. 4c). Finally, avdoralimab also inhibited the increase in IL-6, TNF and CCL2 secretion induced *in vitro* by C5a in monocytes purified from COVID-19 patients and activated with a single strand RNA virus-like

stimulus (Fig. 4f). Avdoralimab appears, thus, suitable for blocking the C5a-C5aR1 axis, which is active during COVID-19. The high levels of C5a observed in COVID-19 do not appear to be a passenger phenomenon, as preliminary efficacy data reported two COVID-19 patients recovering from ARDS following treatment with an anti-C5a blocking mAb (IFX-1)[10]. Furthermore, four patients with severe COVID-19 treated with an anti-C5 mAb (eculizumab), exhibited a drop in circulating inflammatory markers[17]. There are several advantages to blocking C5aR1 rather than other components of the complement cascade. First, blocking C5a or C5aR1 leaves C5b intact and preserves the MAC, which plays a key role in controlling several infections. A loss of the MAC would raise safety concerns in COVID-19, as symptomatic patients often develop comorbid conditions, such as bacterial infections, for which the MAC is required. Second, C5aR1 blockade has the advantage over C5a blockade of having no effect on the second C5a receptor, C5L2. The function of C5L2 remains elusive, but it has been suggested that it can act as a decoy receptor, with anti-inflammatory roles[19].

Our data, highlighting the role of the C5a-C5aR1 axis in the pathogenesis of severe COVID-19, are consistent with several previous observations. Indeed, high C5a levels have also been described in various preclinical models of acute lung disease due to highly pathogenic viruses, such as SARS-CoV-1, H1N1, H5N1 and H7N940[1]. High levels of C5a have also been found in the upper respiratory tract and in serum samples from patients infected with the H1N1 virus[20]. Furthermore, BALF from ARDS patients was found to display robust C5a-dependent chemotactic activity[21]. In a mouse model of MERS-CoV infection, C5a concentrations were high in serum samples and lung tissues[22], and anti-C5aR1 antibody treatment decreased viral replication in lung tissue[22]. In a green monkey model of H7N9 infection, treatment with an anti-C5a antibody significantly decreased the levels of IL-6, IFN-γ, TNF and IL-1β and neutrophil infiltration into the lungs[23]. Overall, C5a inhibition markedly decreased the ALI and systemic inflammation induced by viral infection[24].

In addition, the complement system links innate immunity to coagulation[25,26], and its overactivation could promote thrombotic events in patients with severe COVID-19[27]. Complement blockade may, therefore, prevent thrombosis in affected individuals. Further evidence for the involvement of the complement system in the pathogenesis of severe COVID-19 is also provided by the existence of genetic variants of complement regulatory proteins, such as C1 inhibitor (C1inh) and CD55[28]. C1inh bridges the gap between the complement system and the kallikrein-kinin pathway, which is also activated in COVID-19. In severe COVID-19, SARS-CoV-2 saturates the ACE2 receptors expressed in human airway epithelium[29], resulting in an excess of angiotensin II[30], which, in turn, leads to an excess of kallikrein-kinin that may contribute to tissue injury[30] and the activation of coagulation through the contact system[26]. C1inh downregulates these pathways, but could be overwhelmed by the kinin excess and complement cascade overactivity observed in response to SARS-CoV-2.

The data presented here support a role of the C5a-C5aR1 axis in inflammatory mechanisms underlying ARDS development in patients at early or late stages of SARS-COV-2 infection. As described above, in addition to pneumonia and ARDS, there are data to suggest a role of C5a in other COVID-19-related symptoms, including heart, kidney or endothelial cell dysfunction[14], providing support for the testing of C5a-C5aR1 axis blockade in COVID-19 patients. We suggest that such a blockade may prevent the transition from a localized epithelial disease (non-severe COVID-19) to a diffuse endothelial disease (severe COVID-19) (Extended Figure 4d).

Online content

Any methods, additional references, Nature Research reporting summaries, source data, extended data, supplementary information, acknowledgements, peer review information; details of author contributions and competing interests; and statements of data and code availability are available at https://doi.org/10.1038/s41586-020-2600-6.

1. Wang, R., Xiao, H., Guo, R., Li, Y. & Shen, B. The role of C5a in acute lung injury induced by highly pathogenic viral infections. *Emerging microbes & infections* **4**, e28, https://doi.org/10.1038/emi.2015.28 (2015).
2. Cao, X. COVID-19: immunopathology and its implications for therapy. *Nature reviews. Immunology* **20**, 269-270, https://doi.org/10.1038/s41577-020-0308-3 (2020).
3. Mehta, P. *et al*. COVID-19: consider cytokine storm syndromes and immunosuppression. *Lancet* **395**, 1033-1034, https://doi.org/10.1016/S0140-6736(20)30628-0 (2020).
4. Long, Q. X. *et al*. Antibody responses to SARS-CoV-2 in patients with COVID-19. *Nature medicine*, https://doi.org/10.1038/s41591-020-0897-1 (2020).
5. Guo, R. F. & Ward, P. A. Role of C5a in inflammatory responses. *Annual review of immunology* **23**, 821-852, https://doi.org/10.1146/annurev.immunol.23.021704.115835 (2005).
6. Bosmann, M. & Ward, P. A. Role of C3, C5 and anaphylatoxin receptors in acute lung injury and in sepsis. *Adv Exp Med Biol* **946**, 147-159, https://doi.org/10.1007/978-1-4614-0106-3_9 (2012).
7. Ricklin, D., Hajishengallis, G., Yang, K. & Lambris, J. D. Complement: a key system for immune surveillance and homeostasis. *Nature immunology* **11**, 785-797, https://doi.org/10.1038/ni.1923 (2010).
8. Guo, R. F., Riedemann, N. C. & Ward, P. A. Role of C5a-C5aR interaction in sepsis. *Shock* **21**, 1-7, https://doi.org/10.1097/01.shk.0000105502.75189.5e (2004).
9. Russkamp, N. F. *et al*. Experimental design of complement component 5a-induced acute lung injury (C5a-ALI): a role of CC-chemokine receptor type 5 during immune activation by anaphylatoxin. *FASEB J*: **29**, 3762-3772, https://doi.org/10.1096/fj.15-271635 (2015).
10. Gao, T. *et al*. Highly pathogenic coronavirus N protein aggravates lung injury by MASP-2-mediated complement over-activation. *medRxiv*, 2020.2003.2029.20041962, https://doi.org/10.1101/2020.03.29.20041962 (2020).
11. Liu, J. *et al*. Neutrophil-to-Lymphocyte Ratio Predicts Severe Illness Patients with 2019 Novel Coronavirus in the Early Stage. *medRxiv*, 2020.2002.2010.20021584, https://doi.org/10.1101/2020.02.10.20021584 (2020).
12. Riedemann, N. C. *et al*. Increased C5a receptor expression in sepsis. *The Journal of clinical investigation* **110**, 101-108, https://doi.org/10.1172/JCI15409 (2002).
13. Liao, M. *et al*. Single-cell landscape of bronchoalveolar immune cells in patients with COVID-19. *Nature medicine*, https://doi.org/10.1038/s41591-020-0901-9 (2020).
14. Varga, Z. *et al*. Endothelial cell infection and endotheliitis in COVID-19. *Lancet* **395**, 1417-1418, https://doi.org/10.1016/S0140-6736(20)30937-5 (2020).
15. Teuwen, L. A., Geldhof, V., Pasut, A. & Carmeliet, P. COVID-19: the vasculature unleashed. *Nature reviews. Immunology*, https://doi.org/10.1038/s41577-020-0343-0 (2020).
16. Jayne, D. R. W. *et al*. Randomized Trial of C5a Receptor Inhibitor Avacopan in ANCA-Associated Vasculitis. *Journal of the American Society of Nephrology : JASN* **28**, 2756-2767, https://doi.org/10.1681/ASN.2016111179 (2017).
17. Diurno, F. *et al*. Eculizumab treatment in patients with COVID-19: preliminary results from real life ASL Napoli 2 Nord experience. *European review for medical and pharmacological sciences* **24**, 4040-4047, https://doi.org/10.26355/eurrev_202004_20875 (2020).
18. Lee, H. *et al*. Human C5aR knock-in mice facilitate the production and assessment of anti-inflammatory monoclonal antibodies. *Nature biotechnology* **24**, 1279-1284, https://doi.org/10.1038/nbt1248 (2006).
19. Gerard, N. P. *et al*. An anti-inflammatory function for the complement anaphylatoxin C5a-binding protein, C5L2. *J Biol Chem* **280**, 39677-39680, https://doi.org/10.1074/jbc.C500287200 (2005).
20. Bjornson, A. B., Mellencamp, M. A. & Schiff, G. M. Complement is activated in the upper respiratory tract during influenza virus infection. *Am Rev Respir Dis* **143**, 1062-1066, https://doi.org/10.1164/ajrccm/143.5_Pt_1.1062 (1991).
21. Trujillo, G., *et al*. Cofactor regulation of C5a chemotactic activity in physiological fluids. Requirement for the vitamin D binding protein, thrombospondin-1 and its receptors. *Molecular immunology*, **49**(3), 495–503. 10.1016/j.molimm.2011.09. 024 (2011).
22. Jiang, Y. *et al*. Blockade of the C5a-C5aR axis alleviates lung damage in hDPP4-transgenic mice infected with MERS-CoV. *Emerging microbes & infections* **7**, 77, https://doi.org/10.1038/s41426-018-0063-8 (2018).
23. Sun, S. *et al*. Treatment with anti-C5a antibody improves the outcome of H7N9 virus infection in African green monkeys. *Clinical infectious diseases* **60**, 586-595, https://doi.org/10.1093/cid/ciu887 (2015).
24. Sun, S. *et al*. Inhibition of complement activation alleviates acute lung injury induced by highly pathogenic avian influenza H5N1 virus infection. *American journal of respiratory cell and molecular biology* **49**, 221-230, https://doi.org/10.1165/rcmb.2012-0428OC (2013).
25. Foley, J. H. Examining coagulation-complement crosstalk: complement activation and thrombosis. *Thrombosis research* **141** Suppl 2, S50-54, https://doi.org/10.1016/S0049-3848(16)30365-6 (2016).
26. Thomson, T. M. T., E.; Casis, E.; Paciucci, R. C1-INH and the Contact System in COVID-19-Associated Coagulopathy. *Preprints*, https://doi.org/10.20944/preprints202005.0262.v1 (2020).
27. Magro, C. *et al*. Complement associated microvascular injury and thrombosis in the pathogenesis of severe COVID-19 infection: A report of five cases. *Translational Research*, https://doi.org/10.1016/j.trsl.2020.04.007 (2020).
28. Ramlall, V., Thangaraj, P., Tatonetti, N. P. & Shapira, S. D. Identification of Immune complement function as a determinant of adverse SARS-CoV-2 infection outcome. *medRxiv*, 2020.2005.2005.20092452, https://doi.org/10.1101/2020.05.05.20092452 (2020).
29. Zhang, H. *et al*. Expression of the SARS-CoV-2 ACE2 Receptor in the Human Airway Epithelium. *American journal of respiratory and critical care medicine*, https://doi.org/10.1164/rccm.202003-0541OC (2020).

30. Kuba, K. *et al*. A crucial role of angiotensin converting enzyme 2 (ACE2) in SARS coronavirus-induced lung injury. *Nature medicine* **11**, 875-879, https://doi.org/10.1038/nm1267 (2005).

Explore COVID-19 IPH group

Laura Assante Miranda[3], William Baron[3], Nourhène Belaid[3], Clarisse Caillet[3], Flavien Caraguel[3], Barbara Carrette[3], Florent Carrette[3], Fabien Chanuc[3], Rachel Courtois[3], Aurore Fenis[3], Marilyn Giordano[3], Mathilde Girard-Madoux[3], Marc Giraudon-Paoli[3], Nicolas Gourdin[3], Gwendoline Grondin[3], Franceline Guillot[3], Guillaume Habif[3], Solène Jaubert[3], Julie Lopez[3], Mélanie Le Van[3], Naouel Lovera[3], Marine Mansuy[3], Elodie Bonnet[3], Audrey Sansaloni[3], Annick Reboul[3], Emmanuel Mitry[3], Camille Nekkar-Constant[3], Valentine Péri[3], Paul Ricaut[3], Léa Simon[3], Jean-Baptiste Vallier[3], Marie Vétizou[3] & Robert Zerbib[3]

Explore COVID-19 Marseille Immunopole group

Sophie Ugolini[4], Marion Etiennot[4], Justine Galluso[4], Luc Lyonnet[10], Jean-Marie Forel[10], Laurent Papazian[10], Lionel Velly[10], Baptiste André[10], Antoine Briantais[10], Benoit Faucher[10], Estelle Jean[10], Julie Seguier[10], Veronique Veit[10], Jean-Robert Harlé[10], Boris Pastorino[10], Clémence Delteil[10], Laurent Daniel[10], Jean-Paul Boudsocq[6], Axelle Clerc[6], Emmanuel Delmond[6], Pierre-Olivier Vidal[6], Hélène Savini[6] & Bruno Coutard[2,4]

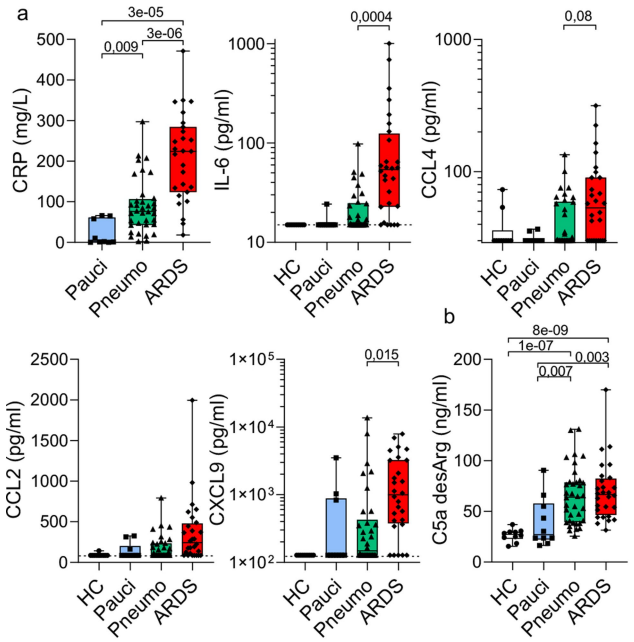

Fig. 1 | Inflammation is associated with a cytokine storm and C5a production in COVID-19 patients. a, Concentrations of CRP, IL-6, CCL4, CCL2 and CXCL9 in plasma from healthy donors (HC) and COVID-19 patients. **b**, Concentration of C5a desArg in plasma of HC and COVID-19 patients. **a**-**b**, HC (white, *n*=10), pauci (blue, *n*=10), pneumo (green, *n*=31 to 34) and ARDS (red, *n*=26 to 28). For CRP and **b** *p*-values were computed using two-tailed Wilcoxon rank-sum tests. For IL-6, CCL4, CCL2 and CXCL9: a global comparison was first performed in which all values were classified into two categories: above or below the LOQ (*p*-values for two-sided Fisher's exact tests demonstrated an increase in the number of values above the LOQ with increasing severity); Fisher tests: $5x10^{-7}$ for IL-6, 0.02 for CCL4, 0.001 for CCL2, $9x10^{-6}$ for CXCL9. A comparison was then performed between pneumonia and ARDS groups, exclusively for values above the LOQ (*p*-values were computed using two-tailed Wilcoxon rank-sum tests). Each symbol represents a single donor. Boxplots represent the median and 25th to 75th percentiles and the whiskers denote the maximum and minimum values.

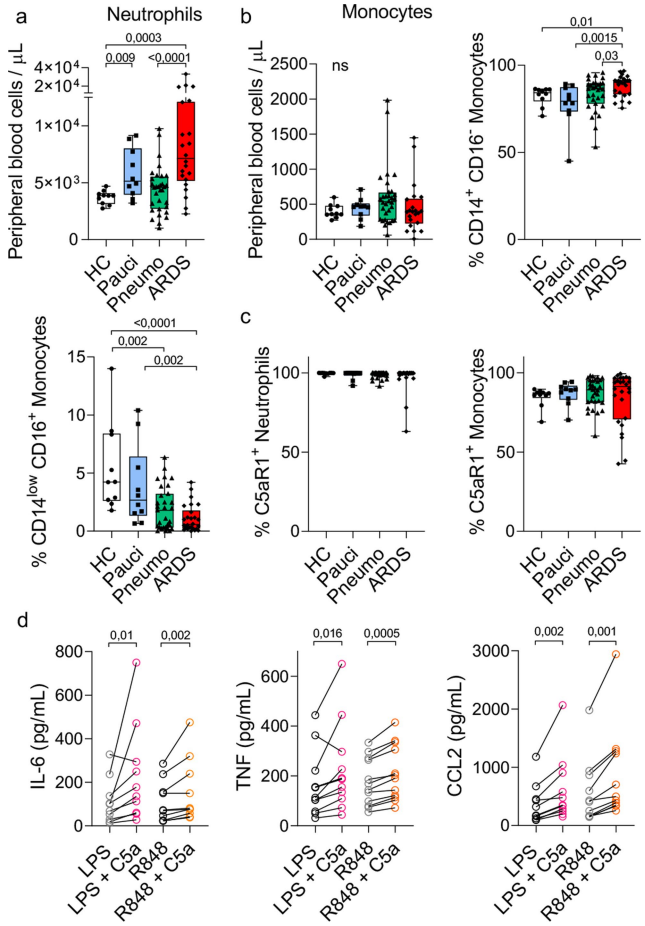

Fig. 2 | C5aR1 is highly expressed on myeloid cells and promotes inflammation. a, Absolute numbers of circulating neutrophils per µL of peripheral blood from healthy donors and COVID-19 patients at T0. **b**, Absolute numbers of circulating total monocytes, and percentages of $CD14^{+}CD16^{-}$ conventional monocytes and $CD14^{low}CD16^{+}$ inflammatory monocytes in the peripheral blood of healthy donors and COVID-19 patients at T0. **c**, Percentage of $C5aR1^{+}$ neutrophils and monocytes in peripheral blood. **a-c**, HC (healthy controls, white, *n*=10), pauci (paucisymptomatic, blue, *n*=10), pneumo (pneumonia, green, *n*=31) and ARDS (red, *n*=26); Each symbol represents a single donor. **d**, IL-6, TNF and CCL2 production by monocytes purified from PBMCs from COVID-19 patients and activated overnight with LPS (0.5 ng/mL) or R848 (50 ng/mL) and C5a (1 µg/mL), when indicated. Each dot represents the mean value obtained from duplicate or triplicate analyses for a single patient (*n*=12 patients). Boxplots represent the median and 25th to 75th percentiles and the whiskers denote the maximum and minimum values. The *p*-values were obtained using two-tailed Wilcoxon rank-sum tests for **a-c** and two-tailed Wilcoxon signed-rank tests for **d**.

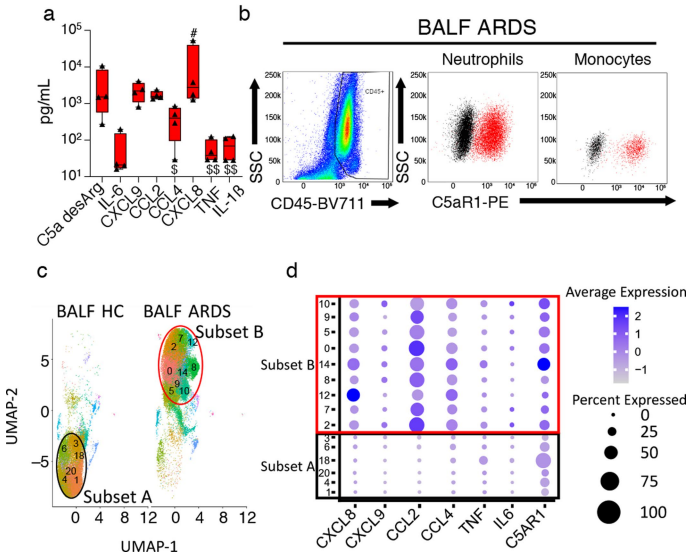

Fig. 3 | C5aR1$^+$ cells and C5a are detected in lung samples from COVID-19 patients. a, Concentration of C5a desArg and IL-6, CXCL9, CCL2, CCL4, IL-8, TNF and IL-1β in the BALF of ARDS patients (*n*=4). # above the detection limit of 52200 pg/mL; $ below the detection limit of 29 pg/mL. **b**, CD45$^+$ immune cell infiltration in BALF from ARDS patients visualized by flow cytometry, and C5aR1 expression (red) vs. FMO (black) staining on CD45$^+$CD14$^-$CD15$^+$CD16$^+$ neutrophils and CD45$^+$CD33$^+$HLADR$^+$CD14$^+$ monocytes in BALF from ARDS patients. The images shown are representative of analyses performed on samples from three ARDS patients. **c**, UMAP of myeloid cell clusters by patient group: healthy controls (*n*=3) and patients with severe COVID-19 (*n*=6). **d**, Dotplot of pro-inflammatory cytokine expression, by cluster.

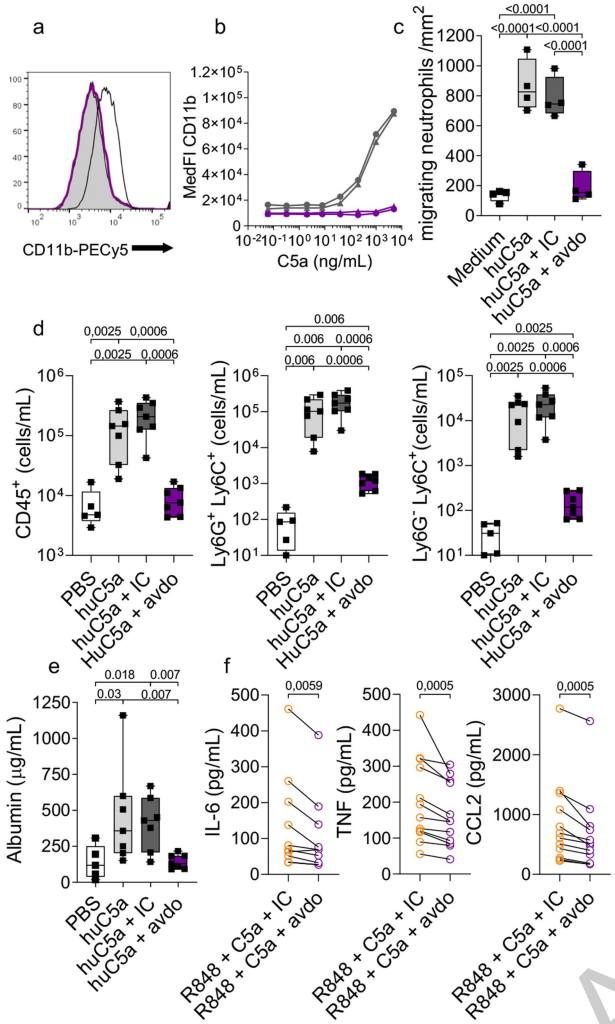

Fig. 4 | Targeting C5aR1 blocks C5a-mediated myeloid cell activation and migration. a, Representative flow cytometry histogram of C5a-mediated CD11b upregulation on whole blood neutrophils, inhibited by avdoralimab. The gray line corresponds to non-activated neutrophils; black line corresponds to C5a-activated neutrophils and purple line corresponds to avdoralimab (30 µg/mL)-treated neutrophils activated with C5a. **b**, CD11b induction through a dose-dependent response to C5a on untreated (gray) or avdoralimab (10 µg/mL)-treated whole-blood neutrophils (purple). Data were obtained from two independent donors. **c**, Migrating neutrophils attracted by C5a. Neutrophils were treated with 10 µg/mL isotype control (dark gray) or avdoralimab (purple) before the induction of migration. Data for neutrophils purified from four healthy donors are shown. **d-e**, BALF was collected from huC5aR1 knock-in mice 18 hours after intranasal instillation of recombinant human C5a. Mice were pretreated with avdoralimab (avdo, purple) or isotype control (IC, dark gray), when indicated. Each symbol represents data from a single mouse, n=5 for PBS group and n=7 for the other groups. Data are representative of 2 experiments. **d**, BALF cell analysis by flow cytometry including $CD45^+$ immune cells, $Ly6C^+Ly6G^+$ neutrophils and $Ly6C^+Ly6G^-$ monocytes. **e**, Albumin concentration in BALF. **f**, Production of IL-6, TNF and CCL2 by monocytes purified from the PBMCs of COVID-19 patients activated by overnight incubation with R848 (50 ng/mL) and C5a (1 µg/mL). Before activation, monocytes were incubated with 20 µg/mL avdoralimab (avdo) or isotype control (IC). Each dot represents the mean value obtained from duplicate or triplicate analyses of a single donor, n=10 for IL-6 and n=12 for TNF and CCL2. Boxplots represent the median and 25th to 75th percentiles and the whiskers denote the maximum and minimum values. The p-values were computed using paired one-way ANOVA for **c**, two-tailed Wilcoxon rank-sum tests for **d-e** and two-tailed Wilcoxon signed-rank tests for **f**.

Methods

Study subjects and clinical considerations

Over a period of one month (03-27-2020 to 04-24-2020), 82 subjects were recruited from three hospitals (Timone and Nord University Hospitals and Laveran Military Hospital, Marseille). Twenty-eight of these patients were on mechanical ventilation for COVID-19-related-ARDS (P/F ratio < 300) (ARDS group), 34 patients required oxygen support at a rate of less than 5 L/min for COVID-19-related pneumonia (pneumonia group). Ten patients had a paucisymptomatic form of COVID-19 compatible with outpatient care (paucisymptomatic group). COVID-19 was diagnosed on the basis of positive SARS-CoV-2 RT-PCR on nasopharyngeal samples and/or typical CT-scan findings[31]. We also included 10 healthy volunteers (control group), with no fever or symptoms in the days before sampling and negative for SARS-CoV-2 RT-PCR. The characteristics of the patients are presented in Supplementary Table 1. Biological samples were first collected within three days of diagnosis and the start of care (T0: < 72 h, early time-point). When possible, the next two time-points for sample collection were located between days 5 and 10 (T1: D5 to D10, intermediate time-point) and after day 10 (T2: > D10, late time-point). Flow cytometry analyses were performed on fresh blood samples (EDTA tubes) and BALFs, immediately after collection. Clinical progression was evaluated between the early and intermediate time points and between the intermediate and late time points. A favorable outcome was defined as weaning from mechanical ventilation (ARDS group) or oxygen support (pneumonia group). Death or multiple organ failure (ARDS group) and admission to the ICU (pneumonia group) were considered unfavorable outcomes. In other cases, patients were considered to be stable.

Ethics approval statement

All the patients (and/or initially their families) provided written informed consent before sampling and for the use of their clinical and biological data. The study protocol was approved on 03-27-2020 by the Committee for the Protection of Persons Ile-de-France III – France (#2020-A00757-32). The pathological examination used in this study was performed secondary to a medical autopsy following COVID-19 related-death, with family agreement and notified to the representative of the Commission on Data Processing and Freedom (MR003 research).

Animals

C57Bl/6J female mice were purchased at Janvier Labs and used between 8 to 12 weeks old. HuC5aR1 KI mice were bred at Charles River Laboratories under specific pathogen-free conditions. Female mice were used at eight to 12 weeks of age and were allowed to acclimate to the housing facility for at least one week. All animal experiments were performed in accordance with the rules of the Innate Pharma ethics committee and were approved by the Ministère de l'Enseignement Supérieur, de la Recherche et de l'Innovation – France (APAFIS#25418-2020051512242806 v2).

Reagent list

DPBS (1X) (14190-094, Gibco); RPMI medium 1640 (1X) (31870-025, Gibco); Sodium pyruvate 100 mM (100X) (11360-039, Gibco); L-glutamine 200 mM (100X) (25030-024, Gibco); Minimum essential medium non-essential amino acids solution (11140-035, Gibco); Trypan blue stain (0.4%) (15250-061, Gibco); Ficoll-Paque PLUS (17-1440-03, GE Healthcare); Fetal bovine serum (F7524, Sigma); Dimethyl sulfoxide (D2650-100ML, Sigma); CD14 microbeads human (130-050-201, Miltenyi); EasySep direct human neutrophil isolation kit (19666, Stemcell); Bovine serum albumin (A9418-100G, Sigma); UltraPure 0.5 M EDTA, pH 8.0 (15575-038, Invitrogen); LPS EK ultrapure (tlrl-peklps, Invivogen); R848 (tlrl-r848, Invivogen); C5a (IPH 1D9 batch 1A, Innate Pharma); C5a (2037-C5-025, R&D Systems); Avdoralimab (Innate Pharma), Isotypic control (Fc-silent hIgG1) (Innate Pharma); CD33- PECF594 clone WM53 (562492, BD Biosciences); CD19-PECy7 clone SJ25C1(557835, BD Biosciences); CD3-BUV496 clone UCHT1 (564809/612940, BD Biosciences); CD15-BV510 clone W6D3 (563141, BD Biosciences); CD45-BV711 clone HI30 (564357, BD Biosciences); CD16-BUV395 clone 3G8 (563785, BD Biosciences); CD14-BUV737 clone M5E2 (564444/612763, BD Biosciences); HLA-DR-AF700 clone L243 (307626, BioLegend); LIVE DEAD NEAR IR (L34976, ThermoFisher); Mouse serum (015-000-120, Jackson ImmunoResearch); CD88 C5aR PE clone S5/1 (344304, BioLegend); Anti-CD16 FITC (556616, BD Biosciences); Anti-CD11b PE-Cy5 (555389, BD Biosciences); U-PLEX kit (N05235A-1, MSD); OptEIATM huC5a ELISA (557965, BD Biosciences); Mouse Albumin ELISA Kit (E99-134, Bethyl Laboratories); Ficoll (11778538, Invitrogen); Dextran (31382, Sigma); Calcein AM (C3100MP, Invitrogen); Fibrinogen (F3879, Sigma); Transwell Fluoroblok 3 µm insert (351151, Corning); EDTA (15575-038, Invitrogen); Sodium azide (71290-100g, Sigma); Optilyse C solution (A11895, Beckman Coulter); CytoFix (554655, BD Bioscience); Avacopan (HY-17627, Clinisciences); Anti-C5a (Innate Pharma); Anti-mouse Ly-6C BV510 clone HK1.4 (128033, BioLegend); Anti-mouse Ly-6G BV786 clone 1A8 (740953, BD Biosciences); Anti-mouse CD45 BUV395 clone 30F11 (564279, BD Biosciences), Anti-mouse CD11b BUV737 clone M1/70 (564443/612800, BD Biosciences); Anti-mouse C5aR1-APC clone 20/70 (130-106-124, Miltenyi Biotec); Anti-human CD88 clone S5/1 (HM2094-100UG, Hycult Biotech); Anti-human CD68 clone KP1 (M0814, Agilent); Anti-human CD163 clone EDHu-1 (MCA1853, BioRad).

SARS-CoV-2 detection by PCR

SARS-CoV-2 RNA was detected by real-time reverse transcription-PCR, as previously described[32].

Seroneutralization assay

Experiments were performed in BSL3 facilities with a clinical isolate of SARS-CoV-2. Virus neutralization tests (VNTs) were performed as previously described[33]. Briefly, VNTs were performed in a 96-well plate, with Vero-E6 cells and a SARS-CoV-2 strain (Ref-SKU:026V-03883 isolated at Charité University, Berlin, Germany; EVA-GLOBAL H2020 project; Grant Agreement 871029). Two-fold serial dilutions of serum samples (final serum dilutions of 1/20 to 1/160) were mixed with 100 $TCID_{50}$ of SARS-CoV2 and dispensed on the confluent cell monolayer. The plates were incubated for four days and examined for the presence (no neutralization) or absence (neutralization) of CPE under an inverted microscope.

Preparation of PBMCs and plasma

Whole blood collected in EDTA tubes was pooled and diluted 1/2 in PBS. PBMCs were isolated by centrifugation on a Ficoll gradient, and 10^7 PBMCs per vial were frozen in freezing medium (90% FCS + 10% DMSO). Plasma was collected from the upper phase of the Ficoll gradient, aliquoted and used for the quantification of soluble factors.

Soluble factor assessment

Human IL-6, CXCL9, CCL2, CCL4, CXCL8, TNF-α and IL-1β levels were analyzed with the U-PLEX kit supplied by MSD (U-PLEX 10-Assay, 96-Well SECTOR Plate, ref: N05235A-1), according to the manufacturer's instructions. The U-PLEX plate was loaded into an MSD instrument to measure the intensity of emitted light, which is proportional to the amount of analyte present in the sample. Circulating C5a-desArg levels were analyzed with the BD OptEIATM huC5a ELISA test. Mouse albumin in BALF was analysed by ELISA (Bethyl). HRP-conjugated secondary Ab was detected by incubation with a peroxidase substrate solution (TMB), and the reaction was stopped by acidification. Plates were read at 450 nm.

Flow cytometry

Blood collected into EDTA tubes was washed in PBS before staining with LiveDead (Thermo Fisher) according to the manufacturer's instructions. Cells were incubated with mouse serum to saturate the

Fc receptors, and were then incubated with the appropriate antibody cocktail. Red blood cells were lysed in Optilyse C Solution (Beckman Coulter), according to the manufacturer's instructions. Cells were fixed in Cell Fix solution (BD), according to the manufacturer's instructions. Data were acquired in an LSRFortessaX20 flow cytometer. The FCS3.0 files obtained were exported from BD FACSDiva software and imported into FlowJo v.10.5.2 (BD Biosciences). Automated compensation was calculated with FACSDiva software and single-stained compensation beads. This compensation matrix was analyzed in detail in FlowJo, by investigating the N-by-N view feature and the pairwise expression of all proteins stained in this study. Fluorescence minus one (FMO) experiments were run before this study, to facilitate optimization of the compensation matrix. We then adjusted the compensation matrix where necessary due to over- or under-compensation by the automatic algorithm.

Immune cell counts

Absolute counts per µL of blood were determined with BD TBNK Trucount™ Tubes. Absolute counts for a particular cell population (A) were obtained by dividing the number of positive cell events (X) by the number of bead events (Y), and then multiplying by the BD Trucount bead concentration (N/V, where N = number of beads per test* and V = test volume). A = X/Y × N/V. The number of positive counts for neutrophils and monocytes was established with the $CD45^{+}SSC^{high}$ and $CD45^{+}SSC^{int}$ gating strategies, respectively.

C5a inhibitors

Avdoralimab is a fully human mutated Fc-silent IgG1 mAb against C5aR1 (US 2020/0017599A1). Anti-C5a mAb is a chimeric mutated Fc silent IgG1 isotype cloned from the sequences of mouse anti-huC5a INab308 (WO2015/140304A1), showing the same variable sequences as IFX-1. C5aR1 antagonist (avacopan) was purchased from Clinisciences (HY-17627).

Neutrophil migration

Neutrophils were isolated from fresh blood by sedimentation in 6% dextran to separate plasma and leukocytes, followed by centrifugation on a Ficoll density gradient. The pellet, containing neutrophils, was recovered, and the red blood cells were lysed by incubation in 0.2% NaCl. Osmotic balance was restored by adding an equal volume of 1.6% NaCl. Isolated neutrophils were loaded with 10 µM calcein AM. Cell density was adjusted before the addition of avdoralimab or its isotype control at a final concentration of 10 µg/mL. Neutrophils were dispensed into the top chamber of a fibrinogen- and BSA-coated Transwell Fluoroblok 3 µm insert. The lower chamber was filled with RPMI 1640 with or without 3 nM C5a (R&D Systems,) and the same antibody was added to the top chamber (avdoralimab, isotype control or PBS). After 30 minutes of incubation at +37 ± 1 °C under an atmosphere containing 5 ± 1% CO_2, images of the lower face of the inserts were acquired on a Biotek Cytation 5 plate-reading microscope, and analyzed with Halo software (Indica Labs), using the CytoNuclear FL module to count the cells that had crossed the membrane.

Neutrophil activation

Various concentrations of avdoralimab were added to the blood samples in culture-treated 96-well U-bottom plates, and incubated for 20 min at 37 °C under an atmosphere containing 5% CO_2. We then added 18 nM human recombinant C5a (R&D Systems) to the samples. Plates were incubated for 20 minutes at 37 °C under an atmosphere containing 5% CO_2. Samples were then stained for flow cytometry analysis with anti-CD16 FITC and anti-CD11b PE-Cy5 antibodies. Erythrocytes were lysed with Optilyse C solution (Beckman Coulter, A11895), according to the manufacturer's protocol, and resuspended in CytoFix (BD Bioscience 554655) for fixation. Cells were then analyzed on a FACS Canto II flow cytometer (BD Biosciences) with FACS Diva software.

Monocyte activation

Monocytes were purified with the $CD14^{+}$ selection kit (Miltenyi). We used 30 000 monocytes to seed 96-well U-bottom plates. Cells were activated by overnight incubation with R848 (50 ng/mL), LPS (0.5 ng/mL) and C5a (1 µg/mL; IPH). In some conditions, monocytes were incubated with avdoralimab (IPH, 20 µg/mL) or its isotype control (IPH, 20 µg/mL) for 30 minutes before stimulation. IL-6, TNF-α and CCL2 were quantified in the supernatant.

Mouse model of lung inflammation

Isoflurane-anesthetized huC5aR1 KI mice received 3.1 µg of recombinant huC5a (R&D) in 40 µL phosphate-buffered saline (PBS), by intranasal instillation. After 18 hours, mice were killed with a lethal dose of ketamine/xylazine cocktail (ketamine 300 mg/kg; xylazine 30 mg/kg). The lungs were flushed with 2 mL 2 mM EDTA in PBS to obtain BALF. After centrifugation (300 x *g*, 5 min, 4 °C), BALF cells were counted and stained for flow cytometry analysis with anti-CD45, anti-Ly6C, anti-Ly6G and anti-CD11b antibodies. For histology analysis, 18 hours after intranasal instillation of huC5a, lungs were fixed in formalin, dissected, embedded in paraffin and sectioned to 5-µm. Sections were dewaxed and stained with hematoxylin and eosin. Slides were finally scanned using a Nanozoomer S60 (Hamamatsu) and examined for evidence of lung damage.

Multiplex immunohistochemistry (OPAL™) staining protocol, image acquisition and data analysis

Multiplexed IHC was performed with a Leica Bond Rx on 5 µm-thick formalin-fixed paraffin-embedded lung tissue sections from individuals with and without COVID-19. Consecutive staining was performed by heat-induced antigen retrieval followed by incubation with primary antibody (anti-C5aR1 clone S5/1 at 1 µg/mL). The signal was amplified and detected with Opal™ polymer horseradish peroxidase and Opal 520 (Akoya Biosciences). The sections were then subjected to heat-induced antibody stripping and incubated with the next antibody (anti-CD163 clone EDHu-1 at 1 µg/mL, detected with Opal 620, and, finally, anti-CD68 clone KP1 at 0.1 µg/mL, detected with Opal 690) and spectral DAPI. All Opal reagents were used at a dilution of 1/150. Slides were finally mounted in ProLong Diamond antifade mounting medium (Thermo Fisher) and scanned with a Vectra Polaris (Akoya Biosciences). Hematoxylin and eosin-stained slides were scanned with a Nanozoomer (Hamamatsu). After spectral deconvolution and whole-slide reconstruction of the multiplexed IHC stained sections, digital pathology methods were used to determine the density of positive cells. All analyses were performed with Halo (Indica Labs) and R.

Transcriptomic analysis

Transcriptomic analyses were performed on previously reported data[13,34,35]{Xiong, 2020 #46}. The RNASeq data for two BALF samples from patients (each in duplicate), three PBMC samples from healthy controls and three PBMC samples from patients were downloaded from the National Genomics Data Center (https://bigd.big.ac.cn/) under accession number PRJCA002326. The RNA-seq data for three BALF samples from healthy controls were downloaded from the SRA database under accession numbers: SRR10571724, SRR10571730, and SRR10571732.

RNASeq pipeline: The reads were mapped to human genome (hg38) release 96 from Ensembl with STAR[68]. PCR replicates mapping to the human genome were removed with the Picard MarkDuplicates program (Broad Institute 2019, http://broadinstitute.github.io/picard/). Gene expression was calculated with featureCounts in the SubReads package (v1.6.4)[36]. TPM (transcripts per million) values were calculated from the raw counts and $\log_2$-transformed. The depth of sequencing of the patient BALF samples was low (< 1 M).

Batch effect correction: we corrected for the batch effect between the datasets for BALF samples from healthy donors and those from patients and PBMC samples with Combat[37], using the model: ~ Batch + Status (Patient or Healthy) + Sample Type (PMBC or BALF). An analysis of differential expression between PBMC samples from healthy donors and those from patients was performed on raw counts with DESeq2[38]. Significance was defined as an adjusted *p*-value <0.05. The metagene *IRAK3, MS4A6A, CD33, CD300C, VCAN, CD1D, CCR1, OAS1, CD163, CD14, FCN1, AIF1, PLA2G7* was used to calculate the macrophage and monocyte transcriptomic signature. The significance of the difference between healthy donors and patients was evaluated in a Wilcoxon test. The single-cell RNASeq data for 12 BALF samples from three healthy donors, three patients with mild COVID-19 and six patients with severe COVID-19 were downloaded from the Gene Expression Omnibus (GEO) database (http://www. https://www.ncbi.nlm.nih.gov/geo) under accession number GSE145926. Quality controls were applied to each cell, for all samples, with the same criteria as for the initial analysis: gene number between 200 and 6,000, UMI count >1,000 and mitochondrial gene percentage < 0.1, with the Seurat package (v3.1.0). After filtering, 63740 cells were validated. As previously described by Liao et al., the filtered gene-barcode matrix was first normalized with 'LogNormalize' methods in Seurat v.3, with default parameters. The top 2,000 variable genes were then identified by the 'vst' method with the Seurat FindVariableFeatures function. The variables 'nCount_RNA' and 'percent.mito' were regressed out in the scaling step and PCA was performed on the top 2,000 variable genes. For the re-analysis presented here, the batch effects across different donors were removed by Harmony[39] and UMAP was performed on the top 50 dimensions for visualizing the cells. Graph-based clustering was performed on the Harmony corrected data, with a resolution of 1.2, and defined major clusters composed of epithelial cells, B and plasma cells, T and NK cells, dendritic cells, monocytes, macrophages and neutrophils. The 50610 myeloid cells were re-integrated and reclustered.

Data analysis and statistics

All statistical analyses were performed with R (version 3.6.1). The ggpubr (version 0.2.5) and lmerTest (version 3.1.2) packages were used for statistical tests. The gtsummary package (version 1.3.0) was used for the clinical table. The sva package (version 3.32.1) was used to correct the batch effect of RNAseq. Packages ggplot2(version 3.2.1) and pheatmap (1.0.12) were used for the graphical representations of RNASeq analyses. The Seurat package (version 3.1.0) was used for all analyses of single-cell RNASeq. For the comparison of groups at timepoint T0, *p*-values were obtained for two-tailed Wilcoxon rank-sum tests. For longitudinal analysis in the pneumonia group, the *p*-values for comparisons of T1 and T0 were obtained in two-tailed Wilcoxon signed-rank tests. No statistical tests were performed for T2 in this group. For the ARDS group, a mixed model was computed, with timepoint as a fixed effect (categorical variable) and patient as a random effect. Confidence intervals and *p*-values were based on the *t*-distribution, with degrees of freedom according to the Kenward-Roger method, and the normality of residuals was verified. Plots were drawn with GraphPad Prism version 8.1.1. Boxplots represent the median and 25th to 75th percentiles and the whiskers denote the maximum and minimum values.

Reporting summary

Further information on research design is available in the Nature Research Reporting Summary linked to this paper.

Data availability

The RNASeq data for two BALF samples from patients (each in duplicate), three PBMC samples from healthy controls and three PBMC samples from patients were downloaded from the National Genomics Data Center (https://bigd.big.ac.cn/) under accession number PRJCA002326. The RNA-seq data for three BALF samples from healthy controls were downloaded from the SRA database under accession numbers: SRR10571724, SRR10571730, and SRR10571732. The single-cell RNASeq data is available from the Gene Expression Omnibus (GEO) database (https://www.ncbi.nlm.nih.gov/geo) under accession number GSE145926. Requests for additional materials or data can be made via email to the corresponding author.

31. Ai, T. et al. Correlation of Chest CT and RT-PCR Testing in Coronavirus Disease 2019 (COVID-19) in China: A Report of 1014 Cases. *Radiology*, **200642**, https://doi.org/10.1148/radiol.2020200642 (2020).
32. Amrane, S. et al. Rapid viral diagnosis and ambulatory management of suspected COVID-19 cases presenting at the infectious diseases referral hospital in Marseille, France, - January 31st to March 1st, 2020: A respiratory virus snapshot. *Travel Med Infect Dis*, **101632**, https://doi.org/10.1016/j.tmaid.2020.101632 (2020).
33. Nurtop, E. et al. Combination of ELISA screening and seroneutralisation tests to expedite Zika virus seroprevalence studies. *Virology journal* **15**, 192, https://doi.org/10.1186/s12985-018-1105-5 (2018).
34. Xiong, Y. et al. Transcriptomic characteristics of bronchoalveolar lavage fluid and peripheral blood mononuclear cells in COVID-19 patients. *Emerging microbes & infections* **9**, 761-770, https://doi.org/10.1080/22221751.2020.1747363 (2020).
35. Dobin, A. et al. STAR: ultrafast universal RNA-seq aligner. *Bioinformatics* **29**, 15-21, https://doi.org/10.1093/bioinformatics/bts635 (2013).
36. Liao, Y., Smyth, G. K. & Shi, W. featureCounts: an efficient general purpose program for assigning sequence reads to genomic features. *Bioinformatics* **30**, 923-930, https://doi.org/10.1093/bioinformatics/btt656 (2014).
37. Johnson, W. E., Li, C. & Rabinovic, A. Adjusting batch effects in microarray expression data using empirical Bayes methods. *Biostatistics* **8**, 118-127, https://doi.org/10.1093/biostatistics/kxj037 (2007).
38. Love, M. I., Huber, W. & Anders, S. Moderated estimation of fold change and dispersion for RNA-seq data with DESeq2. *Genome biology* **15**, 550, https://doi.org/10.1186/s13059-014-0550-8 (2014).
39. Korsunsky, I. et al. Fast, sensitive and accurate integration of single-cell data with Harmony. *Nature methods* **16**, 1289-1296, https://doi.org/10.1038/s41592-019-0619-0 (2019).

Acknowledgements We thank all the healthcare workers involved in the analysis, diagnosis and treatment of patients at AP-HM and Hôpital Laveran, especially Elise Kaspi, Eric Garnotel, Corinne Surcouf, Francois Xavier Le Flem (Bataillon des Marins Pompiers Marseille). We thank all our patients, supporters and families for their confidence in our work. The E.V. laboratory at CIML and Assistance-Publique des Hôpitaux de Marseille is supported by funding from the European Research Council (ERC) under the European Union's Horizon 2020 research and innovation program (TILC, grant agreement No. 694502 and MInfla-TILC, grant agreement No. 875102 - MInfla-Tilc), the *Agence Nationale de la Recherche* including the PIONEER Project (ANR-17-RHUS-0007), MSDAvenir, Innate Pharma and institutional grants awarded to the CIML (INSERM, CNRS, and Aix-Marseille University) and Marseille Immunopole.

Author contributions J.C, F.V. and E.V initiated and designed the research. O.D and E.V. wrote the manuscript with the help of other coauthors. O.D., L.B., J.F. S.C., M-L.T., A.M., P.A., C.P., L.L., W.B., N.B., C.C., B.C., F.C., R.C., A.F., M.G., M.G-M., M.G-P., N.G., G.G., F.G., S.J., J.L., M. L-V., N.L., M.M., C.N-C., V.P., A.R., P.R., J-B.V., M.V., E.B., A.S., A.R., Y.M., E.M., R.Z., L.L., J.G., M.Et., G.H., R.R., L.S., F.C., L.A.M., S.U., B.P., B.C., C.D., L.D. performed the experiments and analyzed and/or interpreted results. J-M.F, L.P., L.V., B.A., A.B., B.F., E.J, J.S., V.V., J-R.H., J.P.B., A.C., E.D., P-O.V., H.S., J.C., N.C.B, M. G., J-M.F., L.P., M.Eb. and N.S. were in charge of patient care and contributed to the discussion of the results. L.B., N.C.B., J.F., S.C., M-L.T. and A.M. equally contributed.

Competing interests O.D., L.B., J.F. S.C., M-L.T., A.M., P.A., E.V. W.B., N.B., C.C., B.C., F.C., R.C., A.F., M.G., M.G-M., M.G-P., N.G., G.G., F.G., S.J., J.L., M. L-V., N.L., M.M., C.N-C., V.P., A.R., P.R., J-B.V., M.V., Y. M., E. M., R. Z., L.A.M., R.R. and F.C. are employees of Innate Pharma. None of the other authors has any competing financial interests to declare.

Additional information

Supplementary information is available for this paper at https://doi.org/10.1038/s41586-020-2600-6.

Correspondence and requests for materials should be addressed to E.V.

Peer review information *Nature* thanks Bart Lambrecht and the other, anonymous, reviewer(s) for their contribution to the peer review of this work.

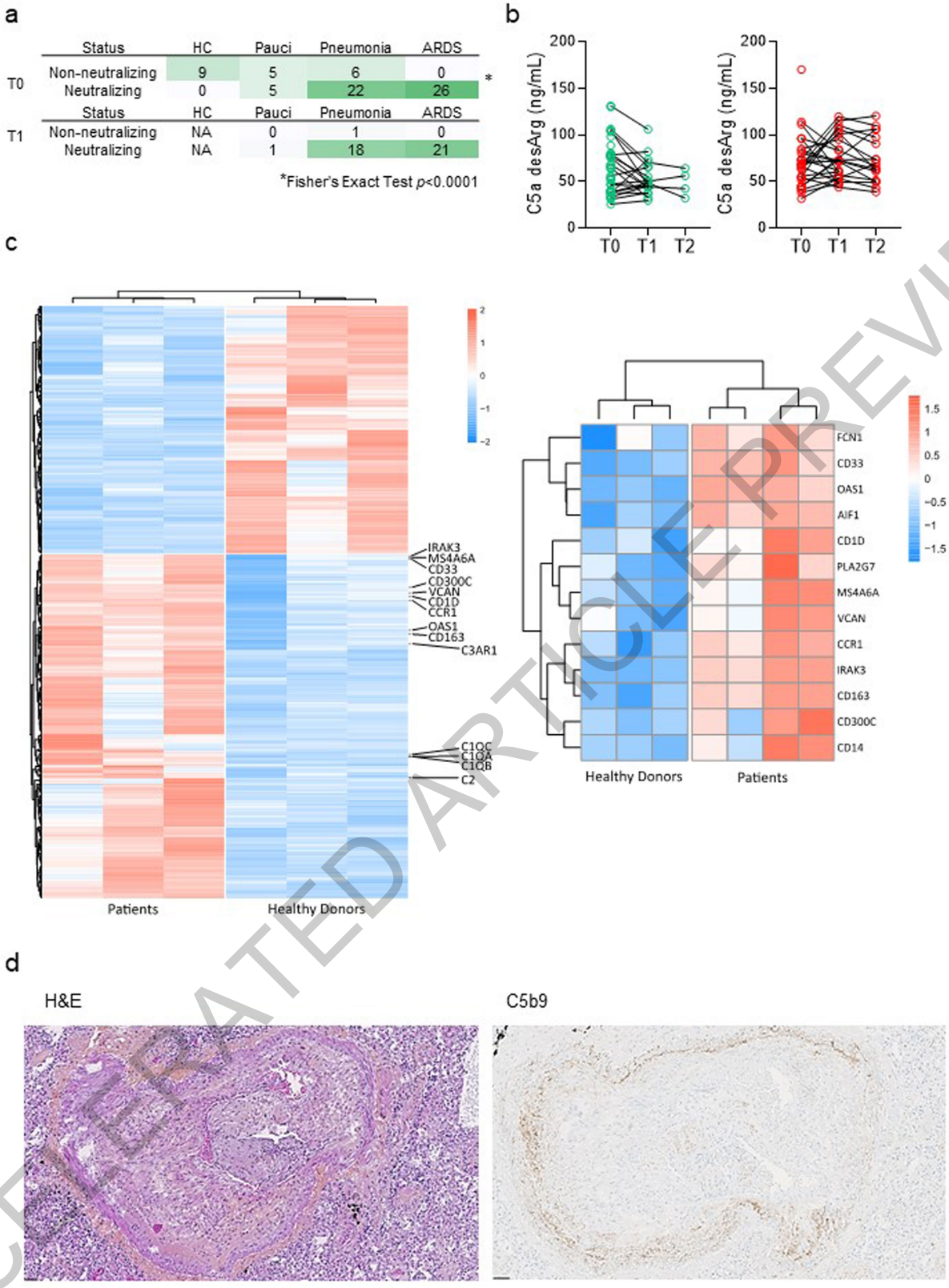

Extended Data Fig. 1 | See next page for caption.

Extended Data Fig. 1 | Immune activation in COVID-19 patients. a, Number of patients for each level of disease severity, classified according to SARS-CoV-2 seroneutralizing status. Biological samples were collected at T0: < 72 h after the start of hospital care; T1: between days 5 and 10. **b**, Concentration of C5a desArg in plasma from pneumonia and ARDS patients followed over time. T0: < 72 h after the beginning of hospital care; T1: between days 5 and 10; T2: > day 10. *p*-values for the comparison of T1 (n=19) and T0 (n=34) in pneumonia group were obtained using two-tailed Wilcoxon signed-rank tests. No statistical tests were performed for T2 (n=4). For ARDS group, a mixed model was computed with timepoint (categorical variable) as a fixed effect and patient as a random effect. n=28 for T0, n=23 for T1 and n=18 for T2. Confidence intervals and *p*-values are based on the *t*-distribution, with degrees of freedom according to the Kenward-Roger method. Each symbol represents a single donor. **c**, Left, Heatmap of genes differentially expressed (logFC >2 & FDR < 5%) between PBMC samples from healthy donors and COVID-19 patients. Right, Heatmap of monocyte and macrophage metagene expression in lung samples from healthy donors and COVID-19 patients. **d**, Three lung samples from deceased patients were obtained and suitable for IHC analysis. Left, H&E staining of obliterating endarteritis lesions in the lungs of a representative COVID-19 patient. Right, C5b9 IHC staining on lung sections of a representative COVID-19 patients, demonstrating complement pathway activation in lung. Scale bar = 50 µm.

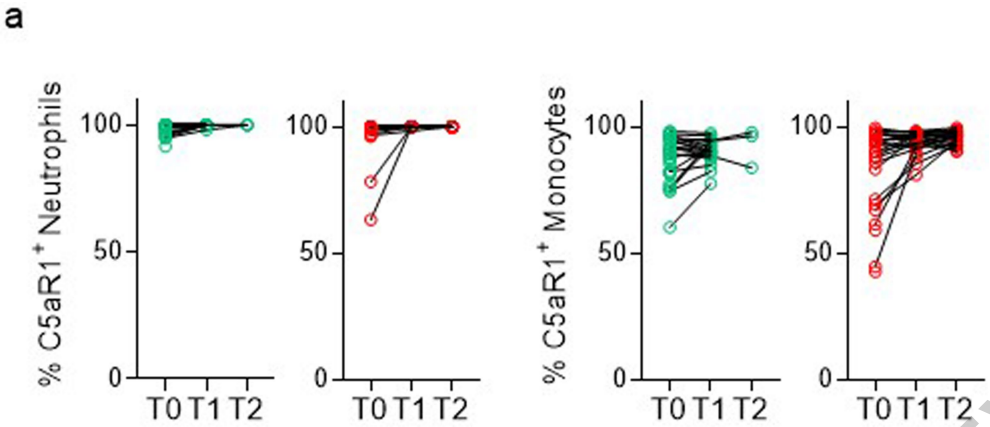

Extended Data Fig. 2 | C5aR1 expression remained stable on myeloid cells during the course of COVID-19. a, % C5aR1-expressing neutrophils and monocytes in pneumonia (green) and ARDS (red) patients followed over time. T0: < 72 h after the start of hospital care; T1: between days 5 and 10; T2: > day 10. For pneumonia group, n= 34 for T0, n=18 (neutrophils) and 21 (monocytes) for T1 and n= 3 for T2. For ARDS group, n=28 for T0, n= 23 for T1 and n= 22 for T2. Each symbol represents a single donor.

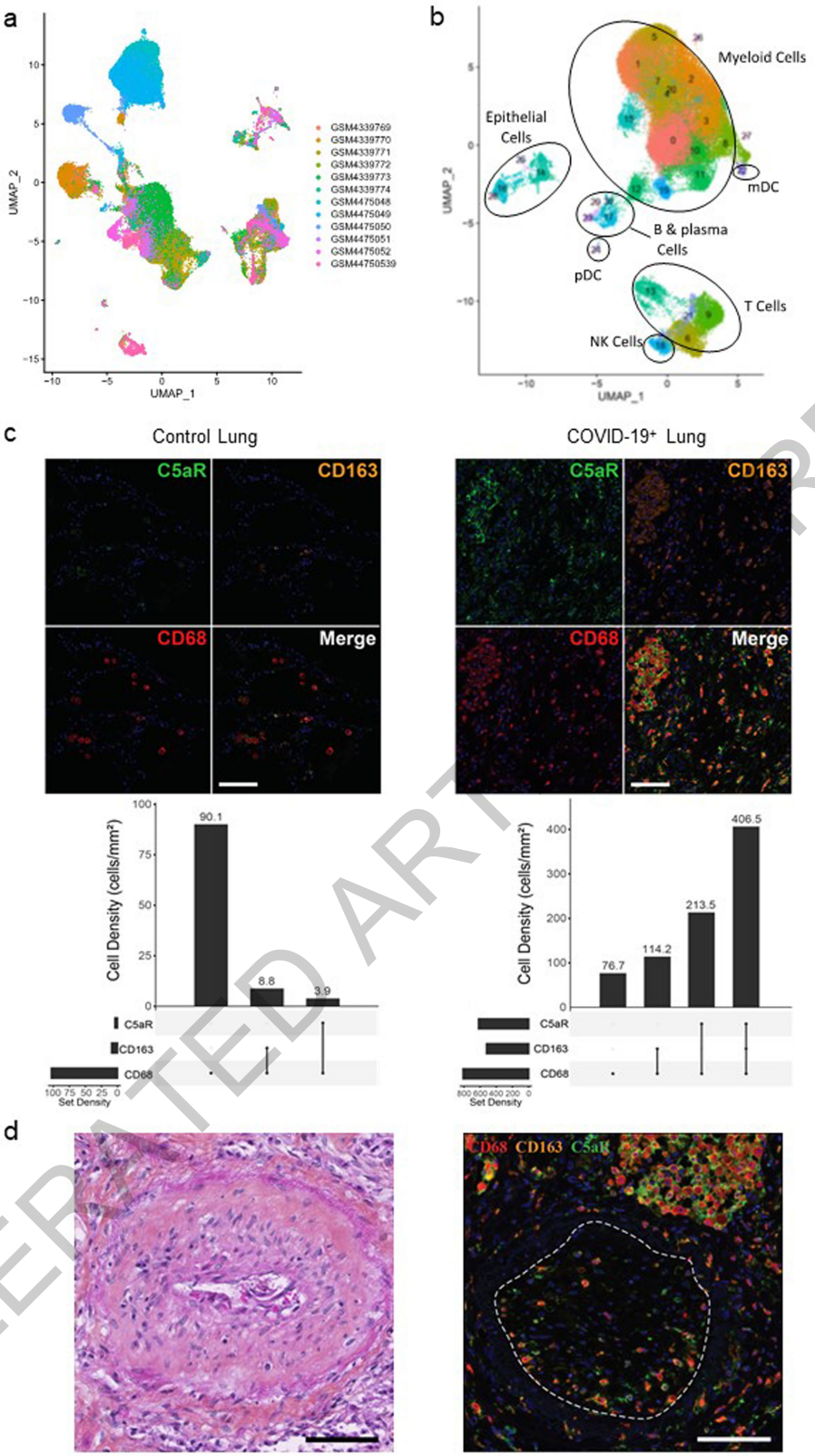

Extended Data Fig. 3 | See next page for caption.

Extended Data Fig. 3 | Myeloid cell analysis in COVID-19 patients. **a-b**, Integration of transcriptomic single-cell data with Harmony. **a**, UMAP projection of donors before integration. **b**, UMAP projection of major cell types and associated clusters after integration by Harmony. **c**, Representative multiplexed IHC staining of C5aR (green), CD68 (red) and CD163 (orange) on lung sections from control or COVID-19 patients among three samples from deceased patients and suitable for IHC analyses. Scale 100 µm. Quantifications represent cell density per mm^2 of multiplexed IHC staining of C5aR1, CD68 and CD163. **d**, Three samples from deceased patients were obtained and suitable for IHC analysis. Endoarteritis lesions were observed in two out of three patients, consistent with previous reports. The patient without endoarteritis lesions did not die from COVID-19. Left, representative H&E staining of obliterating endarteritis lesions in the lungs of COVID-19 patients. Right, representative multiplexed IHC staining of C5aR1 (green), CD68 (red) and CD163 (orange) showing that obliterating endarteritis was frequently associated with $C5aR1^+$ macrophages surrounding the arteries and in the thrombus (white dotted line). Scale 100 µm.

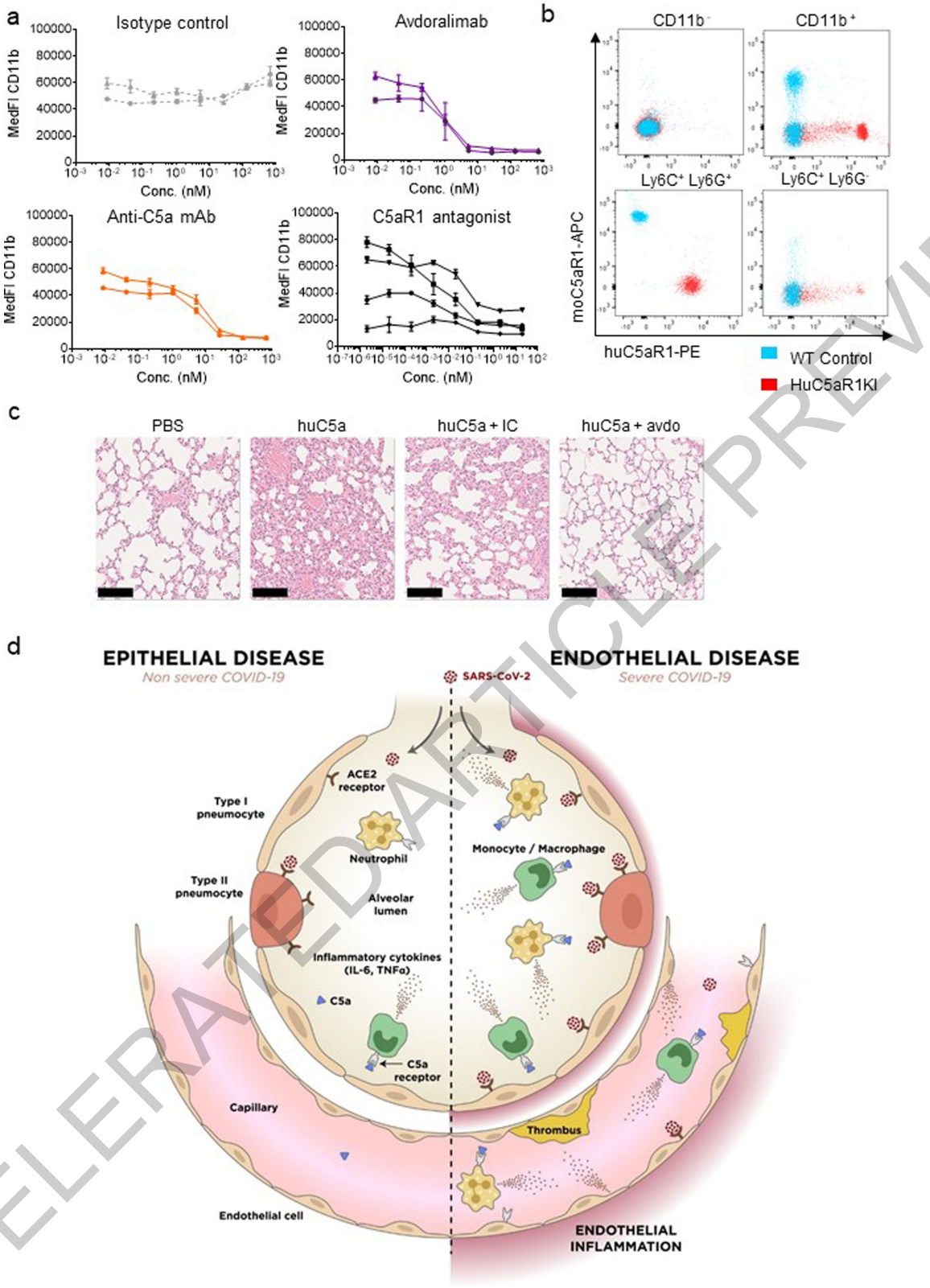

Extended Data Fig. 4 | See next page for caption.

Extended Data Fig. 4 | Targeting C5aR1 to block C5a-mediated myeloid cell activation. a, Analysis of the efficacy of increasing doses of avdoralimab (purple), an anti-C5a mAb (orange), a C5aR1 antagonist (avacopan, black) or IC (gray) for blocking C5a-induced CD11b upregulation on human neutrophils. Each line represents data from a single donor +/- SD from experimental duplicates (PBS) or triplicates (inhibitors). **b**, Comparative expression of mouse C5aR1 (moC5aR1) and human C5aR1 (huC5aR1) on $CD11b^-$ non-myeloid cells, $CD11b^+$ myeloid cells, including $Ly6C^+Ly6G^+$ neutrophils and $Ly6C^+Ly6G^-$ monocytes, from WT (blue) and huC5aR1 KI (red) mice. **c**, H&E staining of lungs from huC5aR1 KI mice treated intranasally with huC5a. Mice were pretreated with avdoralimab (avdo) or isotype control (IC), when indicated. Scale bar =100 µm. Pictures are representative of 2 independent experiments. **d**, A model of C5a involvement in COVID-19: SARS-CoV-2 infects the human airway epithelium via the ACE2 receptors located principally on type II pneumocytes. Left, in non-severe COVID-19, the infection remains confined to the epithelium (epithelial disease), thanks to the efficient action of the immune system. C5a allows the recruitment of myeloid cells without triggering an inflammatory storm, and the virus is eliminated. Right, in severe COVID-19, SARS-CoV-2 escapes the immune system, crosses the epithelium and infect endothelial cells (endothelial disease). The myeloid cells recruited by C5a and endothelial cells release large amounts of inflammatory cytokines. The COVID-19-related cytokine storm and endotheliallitis-associated microthrombosis are triggered. The patient's condition worsens and the virus can infect other organs.

nature research

Corresponding author(s): Prof Eric Vivier

Last updated by author(s): Jul 15, 2020

Reporting Summary

Nature Research wishes to improve the reproducibility of the work that we publish. This form provides structure for consistency and transparency in reporting. For further information on Nature Research policies, see Authors & Referees Editorial Policy Checklist

Statistics

For all statistical analyses, confirm that the following items are present in the figure legend, table legend, main text, or Methods section.

n/a	Confirmed
☐	☒ The exact sample size (*n*
☐	☒ A statement on whether measurements were taken from distinct samples or whether the same sample was measured repeatedly
☐	☒ The statistical test(s) used AND whether they are one- or two-sided *Only common tests should be described solely by name; describe more complex techniques in the Methods section.*
☒	☐ A description of all covariates tested
☐	☒ A description of any assumptions or corrections, such as tests of normality and adjustment for multiple comparisons
☐	☒ A full description of the statistical parameters including central tendency (e.g. means) or other basic estimates (e.g. regression coefficient) AND variation (e.g. standard deviation) or associated estimates of uncertainty (e.g. confidence intervals)
☐	☒ For null hypothesis testing, the test statistic (e.g. *F t r P* *Give P values as exact values whenever suitable.*
☒	☐ For Bayesian analysis, information on the choice of priors and Markov chain Monte Carlo settings
☒	☐ For hierarchical and complex designs, identification of the appropriate level for tests and full reporting of outcomes
☒	☐ Estimates of effect sizes (e.g. Cohen's *d r*

Our web collection on statistics for biologists

Software and code

Policy information about availability of computer code

Data collection	RNASeq pipeline: The reads were mapped to human genome (hg38) release 96 from Ensembl with STAR47. PCR replicates mapping to the human genome were removed with the Picard MarkDuplicates program (Broad Institute 2019, http://broadinstitute.github.io/picard/). Gene expression was calculated with featureCounts function in the SubReads package (v1.6.4)48. TPM (transcripts per million) values were calculated from the raw counts and log2-transformed. Enspire system and software (Perkin Elmer) version 4.13.3005.1482 were used to assess the C5a-desarg concentrations Meso Quickplex SQ 120 system and MSD Workbench 3.0.18 software (MesoScale Discovery) were used to follow the cytokines concentrations.
Data analysis	All statistics analyses were performed using R (version 3.6.1) and GraphPad Prism (version 8.1.1) Packages ggpubr (version 0.2.5) and lmerTest (version 3.1.2) were used for statistical tests and gtsummary (version 1.3.0) for clinical table. Package sva (version 3.32.1) was used to correct the batch effect of RNAseq. Package DESeq2 (version 1.24.0) was used for the differential analysis. Packages ggplot2(version 3.2.1) and pheatmap (1.0.12) were used for the graphical representations of RNASeq analyses in the supplementary figures. Package Seurat (version 3.1.0) was used for all analyses of single-cell RNASeq Graphical representations were performed using GraphPad Prism (version 8.1.1) The FCS3.0 files obtained were exported from BD FACSDiva software version 8.0 and imported into FlowJo v.10.5.2 (BD Biosciences) CytoNuclear FL module from Halo software (Indica Labs) version 3.0.311 was used to count the cells that had crossed the membrane for the neutrophil migration assay All analyses of digital pathology were performed with Halo (Indica Labs) version 3.0.311 and R version 3.6.1.

For manuscripts utilizing custom algorithms or software that are central to the research but not yet described in published literature, software must be made available to editors/reviewers. We strongly encourage code deposition in a community repository (e.g. GitHub). See the Nature Research guidelines for submitting code & software

Data

Policy information about availability of data

All manuscripts must include a data availability statement

- Accession codes, unique identifiers, or web links for publicly available datasets
- A list of figures that have associated raw data
- A description of any restrictions on data availability

PRJCA002326 from https://bigd.big.ac.cn/. SRR10571724, SRR10571730, and SRR10571732 from from the SRA database
GSE145926 from the Gene Expression Omnibus (GEO) database (http://www. https://www.ncbi.nlm.nih.gov/geo)

Field-specific reporting

Please select the one below that is the best fit for your research. If you are not sure, read the appropriate sections before making your selection.

☒ Life sciences ☐ Behavioural & social sciences ☐ Ecological, evolutionary & environmental sciences

For a reference copy of the document with all sections, see nature.com/documents/nr-reporting-summary-flat.pdf

Life sciences study design

All studies must disclose on these points even when the disclosure is negative.

Sample size	As COVID-19 is a new pandemic acute respiratory disease and differences between groups unknown, it was not suitable to estimate the sample size with expected differences. However, we anticipated bigger differences between Pneumo & SARS patients compared to Healthy or Pauci than between the two most severe groups. We decided, thus, to include 10 HC, 10 Pauci, 30-40 Pneumonia and 30-40 SARS patients to be able to detect by t-test a difference of : - One standard deviation (sd) with a power of 80% at a significance level of 5% between HC or Pauci with Pneumo or SARS - 0.6-0.7 sd with a power of 80% at a significance level of 5% between Pneumo and SARS. For in vitro experiments with cells from COVID19 patients: With a sample size of cells isolated from frozen PBMCs of 10 COVID-19 patients, we are able to detect by a paired-t-test a difference of one standard deviation (sd) with a power of 80% at a significance level of 5%. To be sure to get results despite possible technical problems, we included 15 samples of cells isolated from frozen PBMC. For in-vivo mouse experiments: Based on literature, we decided to include 7 mice per group. Using the mean and standard deviation observed in the experiment, we calculated a posteriori the sample size required to achieve a power of 90% at a significance level of 5%. The minimum sample size required to achieve a power of 90% was 6 mice per group.
Data exclusions	Cytometry data were excluded when cell number of population of interest were under 200 events. For In-vitro experiments with patient samples, in the case of not enough cells were harvested to perform the all experimental design, some conditions may lack. One patient was also excluded due to a technical problem.
Replication	Soluble factors analysis and immune cell phenotyping by FACS were performed on a large number of patients (34 pneumonia, 28 ARDS, 10 Paucisymptomatic and 10 healthy controls) to validate reproductibilty of findings BALF analysis were performed from 4 different COVID-19 patients. Three samples from deceased patients suitable for IHC analyses were obtained and processed for H&E and multiplexed IHC staining In vitro experiment of stimulation of COVID-19 monocytes with TLR agonists + C5a +/- avdoralimab was repeated twice and performed on cells from a total of 15 samples from COVID-19 patients and 5 healthy donors. Efficacy of avdoralimab to block CD11b upregulation on neurophils from 3 healthy donors was performed in two independent experiments. Avdoralimab blockade of C5a induced ALI experiment was repeated twice wich 7 mice per group. IHC analysis on lungs from mice upon C5a induced ALI experiment +/- avdoralimab was repeated twice.
Randomization	Human samples were included in groups based on the severity (paucisymptomatic, pneumonia or ARDS) of the patient when recruited. For in vitro experiments, patient samples were selected for high percentages of monocytes in frozen PBMC to allow recovery of enough cells to perform the experiments. As no control was possible untill the end of the experimental procedures, no randomization was performed for in vivo experiments in mice.
Blinding	The goal of our study was to investigate the immune response in COVID-19 patients occuring at different severity stage of the disease. Blinding was not possible as we needed to organize our cohort in 3 different groups.

Behavioural & social sciences study design

All studies must disclose on these points even when the disclosure is negative.

Study description	*Briefly describe the study type including whether data are quantitative, qualitative, or mixed-methods (e.g. qualitative cross-sectional, quantitative experimental, mixed-methods case study).*
Research sample	*State the research sample (e.g. Harvard university undergraduates, villagers in rural India) and provide relevant demographic information (e.g. age, sex) and indicate whether the sample is representative. Provide a rationale for the study sample chosen. For studies involving existing datasets, please describe the dataset and source.*
Sampling strategy	*Describe the sampling procedure (e.g. random, snowball, stratified, convenience). Describe the statistical methods that were used to predetermine sample size OR if no sample-size calculation was performed, describe how sample sizes were chosen and provide a rationale for why these sample sizes are sufficient. For qualitative data, please indicate whether data saturation was considered, and what criteria were used to decide that no further sampling was needed.*
Data collection	*Provide details about the data collection procedure, including the instruments or devices used to record the data (e.g. pen and paper, computer, eye tracker, video or audio equipment) whether anyone was present besides the participant(s) and the researcher, and whether the researcher was blind to experimental condition and/or the study hypothesis during data collection.*
Timing	*Indicate the start and stop dates of data collection. If there is a gap between collection periods, state the dates for each sample cohort.*
Data exclusions	*If no data were excluded from the analyses, state so OR if data were excluded, provide the exact number of exclusions and the rationale behind them, indicating whether exclusion criteria were pre-established.*
Non-participation	*State how many participants dropped out/declined participation and the reason(s) given OR provide response rate OR state that no participants dropped out/declined participation.*
Randomization	*If participants were not allocated into experimental groups, state so OR describe how participants were allocated to groups, and if allocation was not random, describe how covariates were controlled.*

Ecological, evolutionary & environmental sciences study design

All studies must disclose on these points even when the disclosure is negative.

Study description	*Briefly describe the study. For quantitative data include treatment factors and interactions, design structure (e.g. factorial, nested, hierarchical), nature and number of experimental units and replicates.*
Research sample	*Describe the research sample (e.g. a group of tagged Passer domesticus, all Stenocereus thurberi within Organ Pipe Cactus National Monument), and provide a rationale for the sample choice. When relevant, describe the organism taxa, source, sex, age range and any manipulations. State what population the sample is meant to represent when applicable. For studies involving existing datasets, describe the data and its source.*
Sampling strategy	*Note the sampling procedure. Describe the statistical methods that were used to predetermine sample size OR if no sample-size calculation was performed, describe how sample sizes were chosen and provide a rationale for why these sample sizes are sufficient.*
Data collection	*Describe the data collection procedure, including who recorded the data and how.*
Timing and spatial scale	*Indicate the start and stop dates of data collection, noting the frequency and periodicity of sampling and providing a rationale for these choices. If there is a gap between collection periods, state the dates for each sample cohort. Specify the spatial scale from which the data are taken*
Data exclusions	*If no data were excluded from the analyses, state so OR if data were excluded, describe the exclusions and the rationale behind them, indicating whether exclusion criteria were pre-established.*
Reproducibility	*Describe the measures taken to verify the reproducibility of experimental findings. For each experiment, note whether any attempts to repeat the experiment failed OR state that all attempts to repeat the experiment were successful.*
Randomization	*Describe how samples/organisms/participants were allocated into groups. If allocation was not random, describe how covariates were controlled. If this is not relevant to your study, explain why.*
Blinding	

Did the study involve field work? ☐ Yes ☐ No

Field work, collection and transport

Field conditions	*Describe the study conditions for field work, providing relevant parameters (e.g. temperature, rainfall).*
Location	
Access and import/export	*Describe the efforts you have made to access habitats and to collect and import/export your samples in a responsible manner and in compliance with local, national and international laws, noting any permits that were obtained (give the name of the issuing authority, the date of issue, and any identifying information).*
Disturbance	*Describe any disturbance caused by the study and how it was minimized.*

Reporting for specific materials, systems and methods

We require information from authors about some types of materials, experimental systems and methods used in many studies. Here, indicate whether each material, system or method listed is relevant to your study. If you are not sure if a list item applies to your research, read the appropriate section before selecting a response.

Materials & experimental systems

n/a	Involved in the study
☐	☒ Antibodies
☒	☐ Eukaryotic cell lines
☒	☐ Palaeontology
☐	☒ Animals and other organisms
☐	☒ Human research participants
☒	☐ Clinical data

Methods

n/a	Involved in the study
☒	☐ ChIP-seq
☐	☒ Flow cytometry
☒	☐ MRI-based neuroimaging

Antibodies

Antibodies used	Anti-human CD33- PECF594 clone WM53 562492 BD Biosciences (dilution used : 0.32/100) Anti-human CD19-PECy7 clone SJ25C1 557835 BD Biosciences (dilution used : 0.63/100) Anti-human CD3-BUV496 clone UCHT1 564809/612940 BD Biosciences (dilution used : 5/100) Anti-human CD15-BV510 clone W6D3 563141 BD Biosciences (dilution used : 2.5/100) Anti-human CD45-BV711 clone HI30 564357 BD Biosciences (dilution used : 0.3/100) Anti-human CD16-BUV395 clone 3G8 563785 BD Biosciences (dilution used : 2.5/100) Anti-human CD14-BUV737 clone M5E2 564444/612763 BD Biosciences (dilution used : 5/100) Anti-human HLA-DR-AF700 clone L243 307626 BioLegend (dilution used : 2.5/100) LIVE DEAD NEAR IR L34976 ThermoFischer (dilution used : 1/500) Mouse serum 015-000-12 Jackson Immunoresearch (dilution used : 1/10) Anti-human CD88 C5aR PE clone S5/1 344304 BioLegend (dilution used : 2.5/100) U-PLEX kit N05235A-1 Meso Scale Diagnostics OptEIATM huC5a ELISA 557965 BD Biosciences Mouse Albumin ELISA Kit E99-134 Bethyl Laboratories Anti-mouse C5AR1-APC clone 20/70 (dilution used 1:25) Anti-human CD16 FITC 556616 BD Biosciences (dilution used : 2.5/75) Anti-human CD11b PE-Cy5 555389 BD (dilution used : 20/75) Anti-C5a N/A Innate Pharma Anti-mouse Ly-6C BV510 clone HK1 4 128033 BioLegend (dilution used : 1/100) Anti-mouse Ly-6G BV786 clone 1A8 740953 BD Biosciences (dilution used : 1/300) Anti-mouse CD45 BUV395 clone 30F11 564279 BD Biosciences (dilution used : 1/200) Anti-mouse CD11b BUV737 clone M1/70 564443/612800 BD Biosciences (dilution used : 1/300) Anti-human CD88 C5aR clone S5/1 HM2094-100UG Hycult Biotech (concentration : 1µg/ml) Anti-human CD68 clone KP1 M0814 Agilent (concentration : 0.1µg/ml) Anti-human CD163 clone EDHu-1 MCA1853 BIORAD (concentration : 1 µg/mL)
Validation	For Flow cytometry : Titration of each antibodies have been performed under the same conditions as the study (whole blood, 4° C, incubation 30 minutes). The various panels have been tested many times on human (healthy donors and cancer patients) and mouse samples and have been recorded as templates in order to follow a standardization process on BD instrument. For IHC: Primary antibody specificity was validated on formalin-fixed paraffin-embedded cell pellets and tissues. For C5aR, human C5aR-transfected and untransfected cells and kidney tissue were used. For CD68, THP-1 and JURKAT cell lines as well as liver tissue were tested. Finally, SU-DHL-1 and THP-1 cell lines and liver tissue were used for CD163 staining validation.

Eukaryotic cell lines

Policy information about cell lines

Cell line source(s)	*State the source of each cell line used.*
Authentication	*Describe the authentication procedures for each cell line used OR declare that none of the cell lines used were authenticated.*
Mycoplasma contamination	*Confirm that all cell lines tested negative for mycoplasma contamination OR describe the results of the testing for mycoplasma contamination OR declare that the cell lines were not tested for mycoplasma contamination.*
Commonly misidentified lines (See ICLAC	*Name any commonly misidentified cell lines used in the study and provide a rationale for their use.*

Palaeontology

Specimen provenance	*Provide provenance information for specimens and describe permits that were obtained for the work (including the name of the issuing authority, the date of issue, and any identifying information).*
Specimen deposition	*Indicate where the specimens have been deposited to permit free access by other researchers.*
Dating methods	*If new dates are provided, describe how they were obtained (e.g. collection, storage, sample pretreatment and measurement), where they were obtained (i.e. lab name), the calibration program and the protocol for quality assurance OR state that no new dates are provided.*

☐ Tick this box to confirm that the raw and calibrated dates are available in the paper or in Supplementary Information.

Animals and other organisms

Policy information about studies involving animals ARRIVE guidelines

Laboratory animals	C57Bl/6J female mice were purchased at Janvier Labs and used between 8 to 12 weeks old. HuC5aR1 KI mice were bred at Charles River Laboratories under specific pathogen-free conditions. After reception, mice were housed in Innate Pharma animal facilities and had a SOPF (Specific and Opportunist Pathogen Free) health status. Animals were housed in an air-conditioned building. The targeted conditions for animal room environment were as follows: Temperature: 22°C ± 2°C Relative humidity: 40 -75 % Air changes: 15-20 air changes per hour. Both supply and exhaust air are HEPA-filtered. Lighting cycle: 12 hours light/dark daily lighting cycle Caging: Mice were housed as single-sex social groups, in 500 cm2 cages containing between two and five animals. Diet: Rats Mice Hamsters breeding irradiated diet Water: Tap water, sterilized in an autoclave for 20 min at 121 °C, was available ad libitum to each animal via a bottle with a sipper tube. Acclimatization period: The study animals were acclimated to their housing environment for at least 4 days prior to entering the study. Female and male between 7 and 12 weeks old were used for experiments.
Wild animals	No Wild animals were used in our study.
Field-collected samples	No field collected samples were used in the study.
Ethics oversight	All animal experiments were performed in accordance with the rules of the Innate Pharma ethics committee and were approved by the ministere de l'enseignement superieur, de la recherche et de l'innovation – France (APAFIS#25418-2020051512242806 v2).

Note that full information on the approval of the study protocol must also be provided in the manuscript.

Human research participants

Policy information about studies involving human research participants

Population characteristics	We recruited 72 COVID-19 patients with 3 levels of severity: intensive care unit patients with COVID-19-related ARDS, medical unit patients with COVID-19 related pneumonia requiring oxygen support and paucisymptomatic patients. Cohort carateristics: median age 61 years old, female 26% and male 74%, COVID-19 diagnosed by RT PCR, nasopharingeal sampling or Chest CT-Scan. 10 healthy volunteers were also recruited, median age 54 years old, 8 men and 2 women, according to the usual gender distribution of COVID-19. Negativity for SARS-COV-2 was evluated by SARS-CoV-2 RT-PCR and serology analysis.
Recruitment	Over a period of one month (03-27-2020 to 04-24-2020), 82 subjects were recruited from three hospitals (Timone and Nord

Recruitment	University Hospitals and Laveran Military Hospital, Marseille). Twenty-eight of these patients were on mechanical ventilation for COVID-19-related-ARDS (P/F ratio < 300) (ARDS group), 34 patients required oxygen support at a rate of less than 5 L/min for COVID-19-related pneumonia (pneumonia group). Ten patients had a paucisymptomatic form of COVID-19 compatible with outpatient care (paucisymptomatic group). COVID-19 was diagnosed on the basis of positive SARS-CoV-2 RT-PCR on nasopharyngeal samples and/or typical CT-scan findings. We also included 10 healthy volunteers (control group), with no fever or symptoms in the days before sampling and negative for SARS-CoV-2 RT-PCR. The healthy volunteers were recruited in our laboratory and medical units. They were not sick at the time of the samples with no fever, cough or flu syndrome. They didn't take any treatment at the time of sampling. All their COVID-19 serologies were negative. They signed an authorization to participate.
Ethics oversight	The study protocol was approved on 03-27-2020 by the Committee for the Protection of Persons Ile-de-France III – France (#2020-A00757-32)

Note that full information on the approval of the study protocol must also be provided in the manuscript.

Clinical data

Policy information about clinical studies

All manuscripts should comply with the ICMJE guidelines for publication of clinical research CONSORT checklist

Clinical trial registration	N/A
Study protocol	All the patients (and/or initially their families) provided written informed consent before sampling and for the use of their clinical and biological data. The study protocol was approved on 03-27-2020 by the Committee for the Protection of Persons Ile-de-France III – France (#2020-A00757-32). The pathological examination used in this study was performed secondary to a medical autopsy following COVID-19 related-death, with family agreement and notified to the representative of the Commission on Data Processing and Freedom (MR003 research).
Data collection	Biological samples were first collected within three days of diagnosis and the start of care (T0: < 72 h, early time-point). When possible, the next two time-points for sample collection were located between days 5 and 10 (T1: D5 to D10, intermediate time-point) and after day 10 (T2: > D10, late time-point). Flow cytometry analyses were performed on fresh blood samples (EDTA tubes) and BALFs, immediately after collection
Outcomes	N/A

ChIP-seq

Data deposition

☐ Confirm that both raw and final processed data have been deposited in a public database such as GEO

☐ Confirm that you have deposited or provided access to graph files (e.g. BED files) for the called peaks.

Data access links *May remain private before publication.*	*For "Initial submission" or "Revised version" documents, provide reviewer access links. For your "Final submission" document, provide a link to the deposited data.*
Files in database submission	*Provide a list of all files available in the database submission.*
Genome browser session (e.g. UCSC	*Provide a link to an anonymized genome browser session for "Initial submission" and "Revised version" documents only, to enable peer review. Write "no longer applicable" for "Final submission" documents.*

Methodology

Replicates	*Describe the experimental replicates, specifying number, type and replicate agreement.*
Sequencing depth	*Describe the sequencing depth for each experiment, providing the total number of reads, uniquely mapped reads, length of reads and whether they were paired- or single-end.*
Antibodies	*Describe the antibodies used for the ChIP-seq experiments; as applicable, provide supplier name, catalog number, clone name, and lot number.*
Peak calling parameters	*Specify the command line program and parameters used for read mapping and peak calling, including the ChIP, control and index files used.*
Data quality	*Describe the methods used to ensure data quality in full detail, including how many peaks are at FDR 5% and above 5-fold enrichment.*
Software	*Describe the software used to collect and analyze the ChIP-seq data. For custom code that has been deposited into a community repository, provide accession details.*

Flow Cytometry

Plots

Confirm that:

☒ The axis labels state the marker and fluorochrome used (e.g. CD4-FITC).

☒ The axis scales are clearly visible. Include numbers along axes only for bottom left plot of group (a 'group' is an analysis of identical markers).

☒ All plots are contour plots with outliers or pseudocolor plots.

☒ A numerical value for number of cells or percentage (with statistics) is provided.

Methodology

Sample preparation	Blood collected into EDTA tubes was washed in PBS before staining with LiveDead stain according to the manufacturer's instructions. Cells were incubated with mouse serum for 10 minutes at 4°C to saturate the Fc receptor, and were then washed, resuspended in the appropriate antibody cocktail and incubated for 30 minutes at 4°C. Red blood cells were lysed in Optilyse C Solution (Beckman Coulter), according to the manufacturer's instructions. Cells were fixed in Cell Fix solution (BD), according to the manufacturer's instructions.
Instrument	Becton Dickinson LSR Fortessa X20
Software	The FCS3.0 files obtained were exported from BD FACSDiva software and imported into FlowJo v.10.5.2 (BD Biosciences). Automated compensation was calculated with FACSDiva software and single-stained compensation beads. This compensation matrix was analyzed in detail in FlowJo, by investigating the N-by-N view feature and the pairwise expression of all proteins stained in this study. Fluorescence minus one (FMO) experiments were run before this study, to facilitate optimization of the compensation matrix. We then adjusted the compensation matrix where necessary due to over- or under-compensation by the automatic algorithm.
Cell population abundance	Monocytes were purified with positive selection CD14+ kit for in vitro experiment with a mean of purity of 65%. Neutrophils were purified with a ficoll gradient for in vitro experiment with a mean of purity of 78%.
Gating strategy	Neutrophils: Time Gate / Single cells (SSC-A SSC-W) / Living cells (livedead neg) / Leucocytes (CD45+)/ CD45Dim SSCHigh: NeutroEosino/SSC-A SSC-W Single Cells/CD14- CD19-/CD19- CD15+/CD16+ CD45Low Monocytes: Time Gate / Single cells (SSC-A SSC-W) / Living cells (livedead neg) / Leucocytes (CD45+)/ CD45High SSCLow: MonoLymphoBaso/CD33+ CD19-/CD33+ or HLA-DR+/CD14low&hi HLA-DR+/Morpho SSC-A FSC-A Classical Monocytes: Time Gate / Single cells (SSC-A SSC-W) / Living cells (livedead neg) / Leucocytes (CD45+)/ CD45High SSCLow: MonoLymphoBaso/CD33+ CD19-/CD33+ or HLA-DR+/CD14low&hi HLA-DR+/Morpho SSC-A FSC-A /CD14+ CD16- Non-classical Monocytes: Time Gate / Single cells (SSC-A SSC-W) / Living cells (livedead neg) / Leucocytes (CD45+)/ CD45High SSCLow: MonoLymphoBaso/CD33+ CD19-/CD33+ or HLA-DR+/CD14low&hi HLA-DR+/Morpho SSC-A FSC-A /CD14- CD16+

☒ Tick this box to confirm that a figure exemplifying the gating strategy is provided in the Supplementary Information.

Magnetic resonance imaging

Experimental design

Design type	*Indicate task or resting state; event-related or block design.*
Design specifications	*Specify the number of blocks, trials or experimental units per session and/or subject, and specify the length of each trial or block (if trials are blocked) and interval between trials.*
Behavioral performance measures	*State number and/or type of variables recorded (e.g. correct button press, response time) and what statistics were used to establish that the subjects were performing the task as expected (e.g. mean, range, and/or standard deviation across subjects).*

Acquisition

Imaging type(s) — *Specify: functional, structural, diffusion, perfusion.*

Field strength — *Specify in Tesla*

Sequence & imaging parameters — *Specify the pulse sequence type (gradient echo, spin echo, etc.), imaging type (EPI, spiral, etc.), field of view, matrix size, slice thickness, orientation and TE/TR/flip angle.*

Area of acquisition — *State whether a whole brain scan was used OR define the area of acquisition, describing how the region was determined.*

Diffusion MRI ☐ Used ☐ Not used

Preprocessing

Preprocessing software — *Provide detail on software version and revision number and on specific parameters (model/functions, brain extraction, segmentation, smoothing kernel size, etc.).*

Normalization — *If data were normalized/standardized, describe the approach(es): specify linear or non-linear and define image types used for transformation OR indicate that data were not normalized and explain rationale for lack of normalization.*

Normalization template — *Describe the template used for normalization/transformation, specifying subject space or group standardized space (e.g. original Talairach, MNI305, ICBM152) OR indicate that the data were not normalized.*

Noise and artifact removal — *Describe your procedure(s) for artifact and structured noise removal, specifying motion parameters, tissue signals and physiological signals (heart rate, respiration).*

Volume censoring — *Define your software and/or method and criteria for volume censoring, and state the extent of such censoring.*

Statistical modeling & inference

Model type and settings — *Specify type (mass univariate, multivariate, RSA, predictive, etc.) and describe essential details of the model at the first and second levels (e.g. fixed, random or mixed effects; drift or auto-correlation).*

Effect(s) tested — *Define precise effect in terms of the task or stimulus conditions instead of psychological concepts and indicate whether ANOVA or factorial designs were used.*

Specify type of analysis: ☐ Whole brain ☐ ROI-based ☐ Both

Statistic type for inference (See Eklund et al. 2016) — *Specify voxel-wise or cluster-wise and report all relevant parameters for cluster-wise methods.*

Correction

Models & analysis

n/a	Involved in the study
☐	☐ Functional and/or effective connectivity
☐	☐ Graph analysis
☐	☐ Multivariate modeling or predictive analysis

Functional and/or effective connectivity

Graph analysis — *Report the dependent variable and connectivity measure, specifying weighted graph or binarized graph, subject- or group-level, and the global and/or node summaries used (e.g. clustering coefficient, efficiency, etc.).*

Multivariate modeling and predictive analysis — *Specify independent variables, features extraction and dimension reduction, model, training and evaluation metrics.*